Scattering approach to multicolour light forces and self-ordering of polarizable particles

Masterarbeit

zur Erlangung des akademischen Grades
Master of Science (MSc)

an der
Fakultät für Mathematik, Informatik und Physik
der
Leopold-Franzens-Universität Innsbruck

vorgelegt von

Stefan Ostermann

Betreuer der Masterarbeit: Univ.-Prof. Dr. Helmut Ritsch

Innsbruck, im Jänner 2014

Abstract

The dynamics induced by light forces onto polarizable, point-like particles such as atoms, molecules or nanospheres in standing wave light fields is a well studied research topic. Trapping, cooling and pattern formation of particles in such geometries is well understood from the theoretical and experimental point of view.

Even though these configurations offer a wide range of methods to simulate solid state materials at a fundamental level, the formed structures cannot be considered as crystals as they are known from condensed matter physics. This is due to the fact that in contrast to the standing wave case, in nature generally *no* a priory order is given. Pattern formation in this case results from dynamical adjustment of the inter-particle distances and particles settle at distances where the system's energy is minimal. In general this dynamics is more complex than the one realized in standing wave traps.

In this thesis we establish configurations which enable more complex dynamics and couplings of particles compared to the traditional standing wave case by using light fields with different polarizations. Due to the fact that collective coherent scattering of laser light by polarizable point particles creates long range forces, the system's properties can be tailored by choice of injected laser powers, frequencies and polarizations.

The polarizable particles are modelled as infinitesimally thin layers, so called beam splitters, which can reflect, transmit and absorb a certain amount of light. A transfer matrix approach enables us to calculate fields and forces induced by the non-interfering pump fields.

We find long range ordering of particles in a translationally invariant system where inter-particle distances and pattern formation can be tuned by variation of laser frequencies and powers. The observed pattern formation is fundamentally different from the one realized in standing wave potentials.

In a further step, we introduce a setup to induce resonant, long range inter particle coupling between particles trapped in a standing wave trap.

These dynamical effects should be observable in existing experimental setups with effective 1D geometries such as atoms coupled to the field of an optical nanofibre or nanospheres inside a hollow core fibre.

Zusammenfassung

Die durch Lichtkräfte auf polarisierbare, punktförmige Teilchen, wie Atome, Moleküle oder Nanokugeln in Stehwellen-Feldern induzierte Dynamik, ist ein gut erforschtes Feld. Das Fangen beziehungsweise Kühlen und die Strukturbildung von Teilchen in solchen Geometrien ist sowohl von theoretischer als auch von experimenteller Seite gut verstanden.

Obwohl diese Konfigurationen viele Methoden zur Simulation von Festkörpern bereitstellen, können die dabei geformten Strukturen nicht als Kristall definiert werden, wie man es aus der Festkörperphysik kennt. Das liegt daran, dass in der Natur im Gegensatz zum Stehwellenfall a priori keine Ordnung vorgegeben ist. Strukturbildung resultiert in diesem Fall aus dynamischer Anpassung der Abstände zwischen den einzelnen Teilchen, welche dabei an Positionen minimaler Energie gefangen werden. Grundsätzlich ist diese Dynamik komplexer als jene, welche mit Hilfe von Stehwellen-Fallen realisiert wird.

In der vorliegenden Arbeit entwickeln wir Konfigurationen, welche es ermöglichen, komplexere Dynamik und Kopplungen zwischen Teilchen zu erreichen indem Licht mit unterschiedlichen Polarisationen verwendet wird. Aufgrund der Tatsache, dass kollektive kohärente Streuung von Laserlicht an polarisierbaren Punktteilchen langreichweitige Wechselwirkungen generiert, können die Eigenschaften des Systems durch die Wahl der eingestrahlten Intensitäten, Frequenzen und Polarisationen angepasst werden.

Die polarisierbaren Teilchen werden als unendlich dünne Schichten, sogenannten Beam-Splittern, modelliert, welche einen gewissen Anteil an Licht reflektieren, transmittieren und absorbieren können. Ein Transfer-Matrix Ansatz ermöglicht die Berechnung der Felder und der Kräfte, welche durch nichtinterferierende Pump-Felder induziert werden.

Dabei ergibt sich eine weitreichende Ordnung von Teilchen in einem translationsinvarianten System, wo die Abstände zwischen Teilchen beziehungsweise die sich einstellende Ordnung durch die Laser Frequenzen und Intensitäten variiert werden können. Die beobachtete Strukturbildung ist fundamental verschieden von jener in Stehwellen-Potentialen.

In einem weiteren Schritt führen wir eine Konfiguration ein, welche resonante, weitreichende Wechselwirkung zwischen Teilchen in einer Stehwellen-Falle erlaubt.

Die vorhergesagten dynamischen Effekte sollten in bereits existierenden experimentellen Aufbauten mit effektiver 1D Geometrie wie Atome, welche an das Feld einer optischen Nanofaser koppeln, oder Nanokugeln in Hohlfasern, realisierbar sein.

Acknowledgements

First, I would like to thank my supervisor Univ.-Prof. Dr. Helmut Ritsch who offered me the opportunity to work in his research group and gave me a project which quickly caught my interest. All other members of the Ritsch-group Wolfgang, Sebastian, Tobias, Laurin, Raimar, Claudiu, Thomas, Dominik, Valentin, Daniela and especially Matthias, who's suggestions helped me in many ways, deserve my gratitude. I can only assume that working with me was not always easy, but I really enjoyed working with you!

Second, I would like to thank my fellow students who joined me during the last five years and share the same passion for physics. Without you, my studies would not have been of the same quality!

I would also like to express special thanks to the many people who helped me gain energy and clear my mind be it when skiing, mountaineering playing volleyball or tennis.

Furthermore, I also owe a lot to my family, in particular my parents Rudi and Elisabeth who unconditionally encouraged and supported me as well as my sister Verena and my brother Raphael, who always stood behind me.

Another big thank goes to my girlfriend Carmen for respecting me and letting me be who I am! The list of things you did for me would fill a book on its own - thank you!

I am deeply grateful to all the people who supported me even if I cannot name them all. Thank you for contributing to my work in some way or another!

Stefan Ostermann
20th January 2014

Contents

Chapter 1

Introduction

Coherent interference of light scattered from extended ensembles of polarizable particles leads to important modifications of the total force on the particles as well as new inter-particle light forces, even if the light fields are far detuned from any optical resonance [1, 2]. One particularly interesting example are atoms in or close to 1D optical micro structures [3, 4] as e.g. an optical nanofibre, where even a single atom can strongly modify light propagation and forces [5, 6]. In a milestone experiment Rauschenbeutel and co-workers recently managed to trap cold atoms alongside a tapered optical fibre [4] and related setups predict and demonstrate strong back-action and inter-particle interaction [7–9] leading to the formation of periodical self-ordered arrays [10, 11]. Even in free space interesting dynamical effects of collective light scattering were recently predicted and studied in standard 1D optical lattices of sufficient optical density [12, 13].

In this work we extend an existing model [12–15] towards multiple frequencies and polarizations of the fields illuminating the particles. This includes a new class of geometries where crystalline order can be dynamically generated and sustained even without prescribing a standing wave lattice geometry. As a generic example the polarizations of two counter-propagating fields can be chosen orthogonally, so that incident and scattered fields do not directly interfere. Light scattering thus occurs independently for both fields and the forces on the particles can simply be added up. However, any structure forming by the scattering of one field component will be seen by all other fields and thus change their scattering properties and the induced forces. On the one hand this mediates non-linear interaction between the different fields, while on the other hand, it generates inter particle interactions throughout the sample inducing a wealth of non-linear complex dynamical effects. Besides such dynamic self-ordering phenomena we also study the possibilities to induce tailored long range interactions via multicolour illumination and collective scattering of particles trapped in prescribed optical potentials.

The results and effects predicted in this thesis are very general and should be valid for various realization methods. The aim is not to give a detailed calculation for a special experimental setup but to show some interesting effects which could be observed in

several geometries where light fields with orthogonal polarizations can be realized.

This work is organized as follows: In chapter 2 we discuss the basic equations we need to introduce the well-established generalized multiple scattering model used throughout this thesis the so called beam splitter method [12–15]. After some fundamental discussions we will also give a detailed description of this method, and generalize it to support multiple polarizations and frequencies.

In chapter 3, before treating the models marking the central piece of this thesis, we will give a short introduction of possible experimental realization methods.

The chapters 4 and 5 are a more detailed discussion of the results already presented in the preprint [16], which was submitted to New Journal of Physics recently.

In chapter 4 the beam splitter formalism is applied to an orthogonal beam trap consisting of an array of particles irradiated by two counter propagating beams of orthogonal polarization and possibly different wave numbers. For two particles we analytically derive conditions on the pump power ratios and wave numbers to trap or stabilize them at a given separation. These results are then numerically extended to higher particle numbers.

In chapter 5 the usual experimental setups for optical lattices are generalized by an additional beam polarized orthogonally to a prescribed standing wave. We analyse how it perturbs the trapped particles and induces peculiar interaction patterns.

Chapter 2

Fundamental discussion

In this chapter we would like to give an introduction to the basic method used throughout this thesis. The so called beam splitter method states that the propagation of far detuned light through a one dimensional atomic lattice or an array of dielectric membranes can be well described in a plane wave approximation with multiple scattering by a corresponding series of beam splitters [12–15]. A very analogous situation arises when the light is transversely strongly confined by optical structures so that scattering dominantly occurs along a preferred direction.

The fundamental equations to describe the propagation of electromagnetic fields through media are Maxwell's equations, where $\mathbf{E}$ and $\mathbf{B}$ correspond to the electric and magnetic field. The fields $\mathbf{D}$ and $\mathbf{H}$ are defined as $\mathbf{D} = \epsilon\mathbf{E} = \epsilon_0\mathbf{E} + \mathbf{P}$ and $\mathbf{B} = \mu\mathbf{H}$ where $\mathbf{P}$ stands for the polarization density of the material, ϵ [ϵ_0] is the permittivity of the material [of the vacuum] and μ the permeability.

$$\nabla \cdot \mathbf{D} = \rho \tag{2.1a}$$

$$\nabla \cdot \mathbf{B} = 0 \tag{2.1b}$$

$$\nabla \times \mathbf{E} + \frac{\partial \mathbf{B}}{\partial t} = 0 \tag{2.1c}$$

$$\nabla \times \mathbf{H} - \frac{\partial \mathbf{D}}{\partial t} = \mathbf{j} \tag{2.1d}$$

In the following we will always assume no currents or charges, resulting in $\rho = 0$ and $\mathbf{j} = 0$.

From (2.1) the equations which are needed to introduce the beam splitter formalism can be easily calculated. This evaluation marks the first part of this chapter. Before explicitly talking about the beam splitter method itself we introduce the terminology of polarizable media. In this case we distinguish between classical polarizability and atomic polarizability which needs quantum optical treatment. In the third part we give a detailed description of the beam splitter method used in this thesis.

2.1 Basic equations

There are two basic equations known from classical electrodynamics, which are the basis of the beam splitter method used. We will shortly recall how these equations are derived and discuss their meaning in terms of the beam splitter method.

2.1.1 Inhomogeneous Helmholtz equation in 1D

The inhomogeneous Helmholtz equation describes the spacial dynamics of the electric field $E(x,t) = E(x)\exp(-i\omega t)$. It is obtained by the separation of the inhomogeneous wave equation for a polarizable material with polarization density $\mathbf{P}$

$$\Delta\mathbf{E} - \frac{1}{c^2}\frac{\partial^2\mathbf{E}}{\partial t^2} = \mu_0\frac{\partial^2\mathbf{P}}{\partial t^2}. \tag{2.2}$$

Equation (2.2) can easily be obtained by calculating the curl of equation (2.1c) giving

$$\nabla\times(\nabla\times\mathbf{E}) + \frac{\partial}{\partial t}(\nabla\times\mathbf{B}) = \nabla\times(\nabla\times\mathbf{E}) + \mu\frac{\partial}{\partial t}(\nabla\times\mathbf{H}) = 0. \tag{2.3}$$

Together with (2.1d), meaning $(\nabla\times\mathbf{H}) = \frac{\partial\mathbf{D}}{\partial t} = \frac{\partial}{\partial t}(\epsilon_0\mathbf{E}+\mathbf{P})$ and the relation $\nabla\times(\nabla\times\mathbf{E}) = \nabla(\nabla\cdot\mathbf{E}) - \nabla^2\mathbf{E} = -\Delta\mathbf{E}$ we find $(\mu{=}\mu_0)$

$$-\Delta\mathbf{E} + \mu_0\epsilon_0\frac{\partial^2\mathbf{E}}{\partial t^2} + \mu_0\frac{\partial^2\mathbf{P}}{\partial t^2} = 0. \tag{2.4}$$

Defining the speed of light as $c := 1/\sqrt{\mu_0\epsilon_0}$ yields equation (2.2).

Performing a separation ansatz in 1D

$$D(x,t) = D(x)e^{-i\omega t} = (\epsilon_0 E(x) + P(x))\,e^{-i\omega t}, \tag{2.5}$$

results in the purely spatial equation

$$\frac{\partial^2 E(x)}{\partial x^2} + \frac{\omega^2}{c^2}E(x) = -\mu_0\omega^2 P(x). \tag{2.6}$$

This is the so called 1D inhomogeneous Helmholtz equation describing the spatial dynamics of electric fields propagating through dielectric media.

2.1.2 Maxwell stress tensor

Due to the fact that we want to study particles, i.e. atoms or dielectric spheres exposed to electromagnetic radiation, we need to find out how the induced forces onto objects in electromagnetic fields can be calculated. This can be achieved via the Maxwell stress tensor, which will be introduced in this chapter. The derivation and a detailed discussion can be found in [17].

As known from electromagnetism the force onto a charged particle with charge q moving with velocity $\mathbf{v}$ through fields $\mathbf{E}$ and $\mathbf{B}$ can be calculated via the generalized Lorentz force $\mathbf{F}_\mathrm{L} = q(\mathbf{E} + \mathbf{j} \times \mathbf{B})$. If we generalize this force for a finite volume with charge density ρ and current $\mathbf{j}$ this is the so called mechanical force induced by the fields $\mathbf{F}_\mathrm{mech} = \int_V (\rho\mathbf{E} + \mathbf{j} \times \mathbf{B}) d^3x$. The total force onto an object in an electromagnetic field is then given as the sum of mechanical force and field force, where the latter is given by Poynting's theorem $\mathbf{F}_\mathrm{field} = \epsilon_0 \int_V \partial_t(\mathbf{E} \times \mathbf{B}) d^3x$.

Using Maxwell's equations for free space ($\mathbf{P} = 0$) giving the relations $\rho = \epsilon_0 \nabla \cdot \mathbf{E}$ and $\mathbf{j} = \frac{1}{\mu_0} \nabla \times \mathbf{B} - \epsilon_0 \partial_t \mathbf{E}$ the integrator for the mechanical force can be rearranged in the following form

$$\begin{aligned}\epsilon_0 \mathbf{E}(\nabla \cdot \mathbf{E}) + \mathbf{j} \times \mathbf{B} &= \epsilon_0 \mathbf{E}(\nabla \cdot \mathbf{E}) - \mathbf{B} \times \left(\frac{1}{\mu_0} \nabla \times \mathbf{B} - \epsilon_0 \partial_t \mathbf{E} \right) \\ &= \epsilon_0 \left(\mathbf{E}(\nabla \cdot \mathbf{E}) - c^2 \mathbf{B} \times (\nabla \times \mathbf{B}) + \mathbf{B} \times \partial_t \mathbf{E} \right). \end{aligned} \tag{2.7}$$

Using $\mathbf{B} \times \partial_t \mathbf{E} = -\partial_t(\mathbf{E} \times \mathbf{B}) + \mathbf{E} \times \partial \mathbf{B}$, which can be easily verified by applying the product rule, we rewrite equation (2.7) to

$$\begin{aligned} &= \epsilon_0 \left(\mathbf{E}(\nabla \cdot \mathbf{E}) - c^2 \mathbf{B} \times (\nabla \times \mathbf{B}) - \partial_t(\mathbf{E}) \times \mathbf{B}) - \mathbf{E} \times (\nabla \times \mathbf{E}) \right) \\ &= \epsilon_0 \left(\mathbf{E}(\nabla \cdot \mathbf{E}) - \mathbf{E} \times (\nabla \times \mathbf{E}) + c^2 \left(\mathbf{B}(\nabla \cdot \mathbf{B}) - \mathbf{B} \times (\nabla \times \mathbf{B}) \right) \right) \\ &\quad - \epsilon_0 \partial_t(\mathbf{E}) \times \mathbf{B}). \end{aligned} \tag{2.8}$$

We used equation (2.1c) to replace the time derivative of $\mathbf{B}$ in the second term.

The total force onto a polarizable particle is

$$\begin{aligned} \mathbf{F} &= \mathbf{F}_\mathrm{field} + \mathbf{F}_\mathrm{mech} \\ &= \epsilon_0 \int_V \left(\mathbf{E}(\nabla \cdot \mathbf{E}) - \mathbf{E} \times (\nabla \times \mathbf{E}) + c^2 (\mathbf{B}(\nabla \cdot \mathbf{B}) - \mathbf{B} \times (\nabla \times \mathbf{B})) \right). \end{aligned} \tag{2.9}$$

The calculation of the curls and scalar products in equation (2.9) can be easily done by writing the fields in its components (in three dimensions)

$$\begin{aligned} &\begin{pmatrix} E_1 \\ E_2 \\ E_3 \end{pmatrix} \cdot \left[\begin{pmatrix} \partial_{x_1} \\ \partial_{x_2} \\ \partial_{x_3} \end{pmatrix} \cdot \begin{pmatrix} E_1 \\ E_2 \\ E_3 \end{pmatrix} \right] - \begin{pmatrix} E_1 \\ E_2 \\ E_3 \end{pmatrix} \times \begin{pmatrix} \partial_{x_1} \\ \partial_{x_2} \\ \partial_{x_3} \end{pmatrix} \times \begin{pmatrix} E_1 \\ E_2 \\ E_3 \end{pmatrix} \\ &= \begin{pmatrix} \frac{1}{2}\partial_{x_1} E_1^2 + \partial_{x_2} E_1 E_2 + \partial_{x_3} E_1 E_3 - \frac{1}{2}\partial_{x_1} E_2^2 - \frac{1}{2}\partial_{x_1} E_3^2 \\ \partial_{x_1} E_1 E_2 + \frac{1}{2}\partial_{x_2} E_2^2 + \partial_{x_3} E_2 E_3 - \frac{1}{2}\partial_{x_2} E_3^2 - \frac{1}{2}\partial_{x_2} E_1^2 \\ \partial_{x_1} E_1 E_3 + \partial_{x_2} E_2 E_3 + \frac{1}{2}\partial_{x_3} E_3^2 - \frac{1}{2}\partial_{x_3} E_1^2 - \frac{1}{2}\partial_{x_2} E_2^2 \end{pmatrix}. \end{aligned} \tag{2.10}$$

The following pattern for every component $\alpha \in \{1, 2, 3\}$ can easily be read off from equation (2.10)

$$\left[\mathbf{E}(\nabla \cdot \mathbf{E}) - \mathbf{E} \times (\nabla \times \mathbf{E}) \right]_\alpha = \sum_\beta \partial_{x_\beta} \left(E_\alpha E_\beta - \frac{1}{2} \mathbf{E} \cdot \mathbf{E} \delta_{\alpha\beta} \right). \tag{2.11}$$

The same calculation can be done for the **B** fields yielding to the same results.

Defining the Maxwell stress tensor as

$$T_{\alpha\beta} = \epsilon_0 \left[E_\alpha E_\beta + c^2 B_\alpha B_\beta - \frac{1}{2} \left(\mathbf{E} \cdot \mathbf{E} + c^2 \mathbf{B} \cdot \mathbf{B} \right) \delta_{\alpha\beta} \right], \tag{2.12}$$

allows us to calculate the components of the force as

$$F_\alpha = \int_V \sum_\beta \partial_{x_\beta} T_{\alpha\beta} d^3x. \tag{2.13}$$

Making use of the divergence theorem one can show that the force onto objects in electromagnetic fields can be calculated through

$$F_\alpha = \oint_{\mathbf{S}} \sum_\beta T_{\alpha\beta} n_\beta dA. \tag{2.14}$$

2.2 Polarizabilities

As the thesis's title suggests, we study the dynamics of polarizable particles. In this section we would like to give a short introduction to the different origins of polarization. This section should not be seen as a detailed discussion about polarizable media but as a simplified picture to get some insight into the thematics. Generally calculating polarizabilities from first principle is non-trivial and we reduce our considerations to the simplest cases.

First we will introduce a very intuitive picture how dispersive materials are polarized and second we will also show that single atoms can be considered as polarizable particles as well and calculate atomic polarizabilities. In this thesis we focus on linear polarizable media, which holds for many experimentally relevant cases.

2.2.1 Polarizable media

In dielectric media the electric fields do not lead to currents inside the medium like it would be the case for inductors but a polarization density (polarization per volume) **P** is induced as it is already defined in chapter 2.1.1. Now we want to consider which mechanism leads to this polarization and what is happening inside the medium. After putting dielectric media into an electric field single dipoles are induced which add up to a total polarization per volume $\mathbf{P} = N\mathbf{p}$, where **p** is the dipole-moment of the elementary dipoles and N is the number of single dipoles inside the corresponding volume. Generally, one distinguishes between three different mechanisms inducing this polarization [18]:

- The deformation of the orbitals of the material due to the electric field (α_{el})

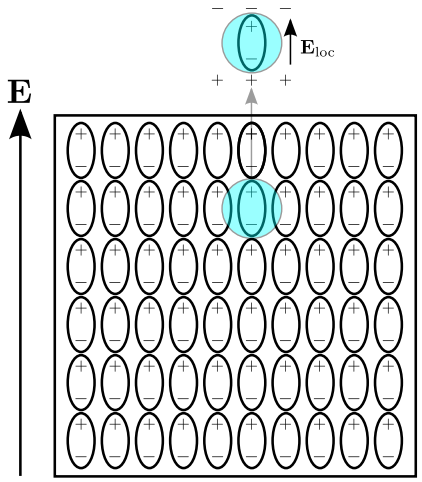

Figure 2.1: Schematic view of the mechanism leading to polarization of dispersive media. The dipoles surrounding every single dipole take influence onto the local electric field $\mathbf{E}_{\mathrm{loc}}$.

- The displacement of ions (α_{ion})
- The orientation of permanent dipoles inside the material in the external field (α_{orient})

All these mechanisms sum up to a total polarizability $\alpha = \alpha_{\mathrm{el}} + \alpha_{\mathrm{ion}} + \alpha_{\mathrm{orient}}$ which in the case of linear polarizable media is the proportionality constant to calculate the induced dipole moment out of the local field at the position of every single elementary dipole via

$$\mathbf{p} = \alpha \mathbf{E}_{\mathrm{loc}}. \tag{2.15}$$

The local field is mainly governed by the material's structure, i.e. the relative positions of the single dipoles. In figure 2.1 a schematic picture of the mechanism described above is shown. Time dependent radiation fields lead to oscillations of the dipoles inside the medium resulting in dipole radiation with the same frequency as the one from the incoming light.

2.2.2 Atomic polarizabilities

In contrast to the materials discussed in the previous chapter, also single atoms act as polarizable particles [19, 20]. Therefore, we consider a two-level system $\{|g\rangle, |e\rangle\}$ in dipole approximation exposed to a classical light field. The dipole approximation contains the assumption that the wavelength of the light imposed on the atom is much larger than the diameter of the atom. The corresponding Hamiltonian is (in rotating wave approximation)

$$H = \hbar\omega_{eg} |e\rangle\langle e| - \mathbf{d}_{eg}\mathbf{E}(\mathbf{r}_A, t) |e\rangle\langle g| - \mathbf{d}_{ge}\mathbf{E}^*(\mathbf{r}_A, t) |g\rangle\langle e| . \tag{2.16}$$

The energy-zero point is set at the level of the ground state and dipole matrix-elements are defined as $\mathbf{d}_{eg} := \langle e| \hat{\mathbf{d}} |g\rangle$ and $\mathbf{d}_{ge} := \langle g| \hat{\mathbf{d}} |e\rangle$. The operator $\hat{\mathbf{d}} = -e\mathbf{r}$ is the quantum mechanical dipole operator.

The second term in (2.16) stands for the absorption of a photon and the third term for emission. The atom is considered to be at position $\mathbf{r}_A$ and the field $\mathbf{E}(\mathbf{r}_A, t)$ is polarized along the chosen quantization direction, i.e. $\mathbf{E}(\mathbf{r}_A, t) = E(\mathbf{r}_A)\mathbf{e}_z e^{-i\omega t} + c.c$, if we assume quantization along the z-axis.

The Hamiltonian (2.16) fulfils the Schrödinger equation $i\hbar\partial_t |\psi(t)\rangle = H |\psi(t)\rangle$, which can be solved using the ansatz

$$|\psi(t)\rangle = a_g(t) |g\rangle + a_e(t) |e\rangle , \tag{2.17}$$

leading to the following system of differential equations for the time dependent amplitudes $a_g(t)$ and $a_e(t)$

$$\partial_t a_g(t) = \frac{i}{\hbar}\mathbf{d}_{ge}\mathbf{E}^*(\mathbf{r}_A, t)a_e(t), \tag{2.18a}$$

$$\partial_t a_e(t) = -i\omega_{eg}a_e(t) + \frac{i}{\hbar}\mathbf{d}_{eg}\mathbf{E}(\mathbf{r}_A, t)a_g(t). \tag{2.18b}$$

Changing to the frame rotating at frequency ω_{eg} allows us to get rid of the transition frequency term in (2.18b). This is performed via the substitution $a_e(t) = \tilde{a}_e(t)e^{-i\omega_{eg}t}$. In the resulting system of equations we can effectively include spontaneous emission via an additional damping term with damping constant γ

$$\partial_t a_g(t) = \frac{i}{\hbar}\mathbf{d}_{ge}\mathbf{E}^*(\mathbf{r}_A, t)a_e(t), \tag{2.19a}$$

$$\partial_t \tilde{a}_e(t) = \frac{i}{\hbar}\mathbf{d}_{eg}\mathbf{E}(\mathbf{r}_A, t)a_g(t) - \gamma\tilde{a}_e(t). \tag{2.19b}$$

This system can easily be solved by first order perturbation theory yielding

$$|\psi(t)\rangle = |g\rangle + \frac{1}{2\hbar}(\mathbf{d}_{eg}\cdot\mathbf{e}_z)E(\mathbf{r}_A)\left[\frac{e^{i(\omega_{eg}+\omega)t}}{\omega_{eg}+\omega-i\gamma} + \frac{e^{i(\omega_{eg}-\omega)t}}{\omega_{eg}-\omega-i\gamma}\right]|e\rangle . \tag{2.20}$$

The induced atomic dipole moment can now be calculated via the expectation value $\mathbf{p}(\mathbf{r}_A, t) = \langle\psi(t)| \hat{\mathbf{d}} |\psi(t)\rangle$ which leads us to

$$\begin{aligned}
\mathbf{p}(\mathbf{r}_A, t) = {} & \frac{1}{2\hbar}E(\mathbf{r}_A)\left[\frac{e^{i(\omega_{eg}+\omega)t}}{\omega_{eg}+\omega-i\gamma} + \frac{e^{i(\omega_{eg}-\omega)t}}{\omega_{eg}-\omega-i\gamma}\right]\mathbf{d}_{ge}(\mathbf{d}_{eg}\cdot\mathbf{e}_z)e^{-i\omega_{eg}t} + \\
& + \frac{1}{2\hbar}E(\mathbf{r}_A)\left[\frac{e^{i(\omega_{eg}+\omega)t}}{\omega_{eg}+\omega-i\gamma} + \frac{e^{i(\omega_{eg}-\omega)t}}{\omega_{eg}-\omega-i\gamma}\right]^*\mathbf{d}_{eg}(\mathbf{d}_{ge}\cdot\mathbf{e}_z)e^{i\omega_{eg}t} \\
= {} & \frac{1}{2\hbar}E(\mathbf{r}_A)\mathbf{d}_{ge}(\mathbf{d}_{eg}\cdot\mathbf{e}_z) \\
& \left[\frac{e^{i\omega t}}{\omega_{eg}+\omega-i\gamma} + \frac{e^{-i\omega t}}{\omega_{eg}-\omega-i\gamma} + \frac{e^{-i\omega t}}{\omega_{eg}+\omega+i\gamma} + \frac{e^{i\omega t}}{\omega_{eg}-\omega+i\gamma}\right] \\
=: {} & E(\mathbf{r}_A)\left[\alpha^*(\omega)e^{i\omega t} + \alpha(\omega)e^{-i\omega t}\right]\mathbf{e}_z = \alpha(\omega)E(\mathbf{r}_A)\mathbf{e}_z e^{-i\omega t} + c.c. .
\end{aligned} \tag{2.21}$$

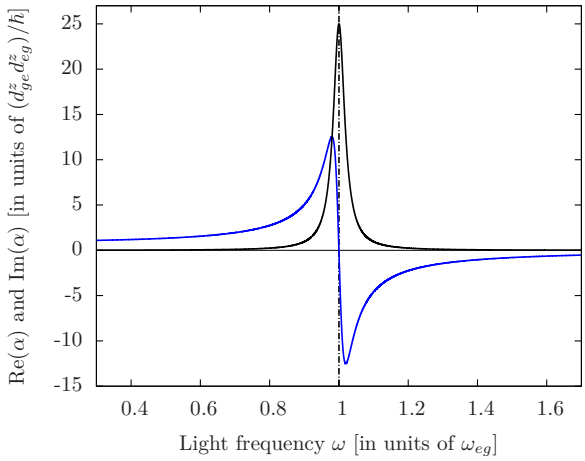

Figure 2.2: Frequency dependence of the real part (blue curve) and imaginary part (black curve) of the atomic polarizability α from equation (2.23).

where we defined the atomic polarizability tensor as $(k, l \in 1, 2, 3)$

$$\alpha_{kl}(\omega) := \frac{d^k_{ge} d^l_{eg}}{2\hbar} \left[\frac{1}{\omega_{eg} + \omega + i\gamma} + \frac{1}{\omega_{eg} - \omega - i\gamma} \right]. \tag{2.22}$$

Due to the fact that we chose the quantization axis in z-direction and the electric field is polarized parallel to this axis, we are able to reduce the tensor polarizability to a scalar quantity $(d^3 \equiv d^z)$

$$\begin{aligned} \alpha(\omega) &= \frac{d^z_{ge} d^z_{eg}}{\hbar} \left[\frac{\omega_{eg}(\omega^2_{eg} - \omega^2)}{(\omega^2 - \omega^2_{eg})^2 + 4\gamma^2} + i \frac{2\gamma\omega\omega_{eg}}{(\omega^2 - \omega^2_{eg})^2 + 4\gamma^2} \right] \\ &= \mathrm{Re}(\alpha) + \mathrm{Im}(\alpha). \end{aligned} \tag{2.23}$$

Figure 2.2 shows the plot of the real and imaginary part of the atomic polarizability given in (2.23). Obviously the real part is zero if $\omega = \omega_{eg}$ and the imaginary part has its maximum at this point. Generally, the real part corresponds to dissipative effects where the imaginary part stands for spontaneous emission.

Writing the induced atomic dipole moment in complex notation, i.e. $\mathbf{p}(\mathbf{r}_A, t) = p(\mathbf{r}_A)\mathbf{e}_z e^{-i\omega t} + c.c.$ and comparing coefficients in equation (2.21) results in the linear relation

$$\tilde{\mathbf{p}}(\mathbf{r}_A) = \alpha(\omega)\tilde{\mathbf{E}}(\mathbf{r}_A), \tag{2.24}$$

where we defined the two vectors $\tilde{\mathbf{p}}(\mathbf{r}_A) := p(\mathbf{r}_A)\mathbf{e}_z$ and $\tilde{\mathbf{E}}(\mathbf{r}_A) := E(\mathbf{r}_A)\mathbf{e}_z$.

Finally we notice that a time dependent electric field with frequency ω induces a harmonically oscillating dipole with the same oszillation frequency, cf. equation (2.21).

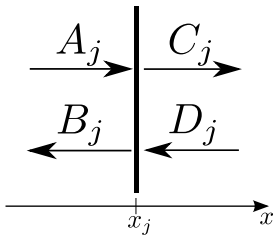

Figure 2.3: Naming convention for the amplitudes at the j^{th} beam splitter. x_j defines the position of the j^{th} beam splitter

2.3 Beam splitter method

On the basis of the last chapters we are now able to introduce the central method used in this thesis: the beam splitter method. This is a semi-classical and one-dimensional model description of light scattering by linear polarizable particles. It allows us to describe the propagation of light through slices of dispersive media or atoms in one dimension. In this chapter we would like to give a short introduction to the basic properties of this method. Further reading can be found in publications on related topics [12, 13, 15, 21].

Considering the beam splitter method, every single dipole in the array acting as a light scatterer is modelled as a so called beam splitter, which can transmit, absorb and reflect a certain amount of light. We use the convention introduced in [15] namely that the incoming amplitudes on the j^{th} beam splitter are named like shown in figure 2.3.

2.3.1 Definition of the transfer matrices

Let us first consider a single beam splitter at position x_j which is illuminated from both left and right sides with monochromatic light $E(x,t) = E(x)\exp(-i\omega t)$. The spatial dynamics of this field is then described by the 1D Helmholtz equation (2.6). The polarization density reads

$$P(x) = \eta\alpha\delta(x - x_j)E(x), \tag{2.25}$$

where η stands for the area density of particles combined to a single beam splitter, $k = \omega/c$ is the wave number and α the polarizability as discussed in chapter 2.2. Here we restrict ourselves to scalar polarizabilities, for a generalization of the beam splitter method to multi-level atoms we refer to a work by Xuereb et al. [22].

If we consider an array with N beam splitters at positions $x_1, ..., x_N$ and define the dimensionless parameter $\zeta := k\eta\alpha/(2\varepsilon_0)$ the spatial dynamics is given via

$$\left(\partial_x^2 + k^2\right) E(x) = -2k\zeta E(x) \sum_{j=1}^{N} \delta(x - x_j). \tag{2.26}$$

The solution of equation (2.26) between two beam splitters, $x \in (x_j, x_{j+1})$ reads

$$E(x) = C_j e^{ik(x-x_j)} + D_j e^{-ik(x-x_j)} \equiv A_{j+1} e^{ik(x-x_{j+1})} + B_{j+1} e^{-ik(x-x_{j+1})}. \tag{2.27}$$

The amplitudes A_j, B_j left and C_j, D_j right of the beam splitter at the position x_j are related by the linear transformation matrix M_{BS}.

The constant $\zeta \in \mathbb{C}$ is the fundamental parameter to describe the interaction between the atom and the light field. Generally, the real part $\mathrm{Re}(\zeta)$ corresponds to dissipative effects while the imaginary part $\mathrm{Im}(\zeta)$ accords to spontaneous emission. This can be easily understood via equation (2.23). As for atoms the following relation for the real part of ζ applies

$$\mathrm{Re}(\zeta) > 0, \text{ for } \omega < \omega_{eg}, \tag{2.28a}$$
$$\mathrm{Re}(\zeta) < 0, \text{ for } \omega > \omega_{eg}. \tag{2.28b}$$

The imaginary part $\mathrm{Im}(\zeta)$ is always positive, cf. figure 2.2.

If we want to treat macroscopic objects like silicon beads using the beam splitter method, the real part of ζ stands for light which is reflected back into the light mode, while the imaginary part describes light that is absorbed inside the medium.

To derive the transfer matrix we consider a single beam splitter at position x_j. The spatial components of the fields left and right of this j^th beam splitter are given by

$$E_j(x) = \begin{cases} A_j e^{ik(x-x_j)} + B_j e^{-ik(x-x_j)}, & \text{for } x < x_j \\ C_j e^{ik(x-x_j)} + D_j e^{-ik(x-x_j)}, & \text{for } x > x_j. \end{cases} \tag{2.29}$$

Of course these fields need to fulfil the continuity condition at position x_j, $E_j(x \to x_j^-) = E_j(x \to x_j^+)$, where $+$ and $-$ stands for the limit performed from the right and the left side. In contrast to that, the derivatives of the field are continuous but not differentiable at the beam splitter position x_j as the following calculation shows. We integrate equation (2.26) over an interval of length 2ϵ ($\epsilon \ll 1$) around x_j.

$$\int_{-\epsilon}^{\epsilon} \left(\partial_x^2 + k^2\right) E_{l,r}(x)dx = -2k\zeta \underbrace{\int_{-\epsilon}^{\epsilon} \delta(x-x_j) E_{l,r}(x)dx}_{E_{l,r}(x=x_j)}$$

$$\int_{-\epsilon}^{\epsilon} \partial_x^2 E_{l,r}(x)dx + k^2 \int_{-\epsilon}^{\epsilon} E_{l,r}(x)dx = -2k\zeta E_{l,r}(x=x_j)$$

$$\partial_x E_{l,r}(\epsilon) - \partial_x E_{l,r}(-\epsilon) + k^2 \int_{-\epsilon}^{\epsilon} E_{l,r}(x)dx = -2k\zeta E_{l,r}(x=x_j)$$

$$\lim_{\epsilon\to 0} \left[\partial_x E_{l,r}(\epsilon) - \partial_x E_{l,r}(-\epsilon)\right] + \underbrace{\lim_{\epsilon\to 0} k^2 \int_{-\epsilon}^{\epsilon} E_{l,r}(x)dx}_{\longrightarrow 0} = -2k\zeta E_{l,r}(x=x_j)$$

$$\Longrightarrow \partial_x E(x \to x_j^+) - \partial_x E(x \to x_j^-) = -2k\zeta E(x=x_j)$$

In summary, the boundary conditions for the fields are as follows

$$E_l(x \to x_j^-) = E_r(x \to x_j^+), \tag{2.30a}$$
$$\partial_x E(x \to x_j^-) - \partial_x E(x \to x_j^+) = 2k\zeta E(x = x_j). \tag{2.30b}$$

We used the naming convention that the fields on the left side ($x < x_j$) of the beam splitter are the ones with index l and the ones on the right side ($x > x_j$) are the ones with index r.

The field amplitudes are connected via the scattering matrix

$$\begin{pmatrix} B_j \\ C_j \end{pmatrix} = \begin{pmatrix} \mathfrak{r}_l & \mathfrak{t}, \\ \mathfrak{t} & \mathfrak{r}_r, \end{pmatrix} \begin{pmatrix} A_j \\ D_j \end{pmatrix}. \tag{2.31}$$

We assumed different reflection coefficients for light from the left and the right side, $\mathfrak{r}_l$ and $\mathfrak{r}_r$ but we will show that for a single beam splitter $\mathfrak{r}_l = \mathfrak{r}_r$. For higher numbers of beam splitters this equality will no longer be true.

Rearranging (2.31) leads us to the definition of the transfer matrix

$$\begin{pmatrix} C_j \\ D_j \end{pmatrix} = \frac{1}{\mathfrak{t}} \begin{pmatrix} \mathfrak{t}^2 - \mathfrak{r}_l\mathfrak{r}_r & \mathfrak{r}_r \\ -\mathfrak{r}_l & 1 \end{pmatrix} \begin{pmatrix} A_j \\ B_j \end{pmatrix}. \tag{2.32}$$

Using the boundary conditions (2.30) we are now able to find out how the reflection and transmission coefficients, $\mathfrak{r}$ and $\mathfrak{t}$, are connected with the parameter ζ. For light from the left side, the incoming, reflected and transmitted fields have the form

$$E_{\text{in}} = A_j e^{ik(x-x_j)}, \tag{2.33a}$$
$$E_{\text{trans}} = \mathfrak{t} A_j e^{ik(x-x_j)}, \tag{2.33b}$$
$$E_{\text{refl}} = \mathfrak{r}_l A_j e^{-ik(x-x_j)}. \tag{2.33c}$$

Setting the fields (2.33) into (2.30a) leads us to the first condition for the reflection and transmission coefficients

$$\begin{aligned} A_j + \mathfrak{r}_l A_j &= \mathfrak{t} A_j, \\ 1 + \mathfrak{r}_l &= \mathfrak{t}, \end{aligned} \tag{2.34}$$

and calculating (2.30b) for the fields (2.33) results in

$$\begin{aligned} \lim_{x \to x_j^-} \partial_x (A_j e^{ik(x-x_j)} + \mathfrak{r}_l A_j e^{-ik(x-x_j)}) - \lim_{x \to x_j^+} \partial_x \mathfrak{t} A_j e^{ik(x-x_j)} &= 2k\zeta A_j (1 + \mathfrak{r}) \\ ik - ik\mathfrak{r}_l - ik\mathfrak{t} &= 2k\zeta(1 + \mathfrak{r}_l). \end{aligned} \tag{2.35}$$

Of course the same calculation can be done for light coming from the right side. In this case $\mathfrak{r}_l$ has to be replaced by $\mathfrak{r}_r$ in (2.34) and (2.35). From the equations (2.34)

and (2.35) the following relations can be found

$$\mathfrak{r} \equiv \mathfrak{r}_l = \mathfrak{r}_r = \frac{i\zeta}{1 - i\zeta}, \tag{2.36a}$$

$$\mathfrak{t} = \frac{1}{1 - i\zeta}. \tag{2.36b}$$

The transfer matrix (2.32) can be rewritten by using (2.36) and we get

$$\begin{pmatrix} C_j \\ D_j \end{pmatrix} = \begin{pmatrix} 1 + i\zeta & i\zeta \\ -i\zeta & 1 - i\zeta \end{pmatrix} \cdot \begin{pmatrix} A_j \\ B_j \end{pmatrix} =: M_{BS} \cdot \begin{pmatrix} A_j \\ B_j \end{pmatrix}. \tag{2.37}$$

This is the transfer matrix for a single beam splitter.

Arrays of beam splitters can now be described by the total transfer matrix which is obtained by matrix multiplication of the transfer matrices for every single beam splitter. Propagation between the beam splitters can be described by a propagation matrix which can be read off from (2.27)

$$\begin{aligned} \begin{pmatrix} A_{j+1} \\ B_{j+1} \end{pmatrix} &= \begin{pmatrix} e^{ik(x_{j+1} - x_j)} & 0 \\ 0 & e^{-ik(x_{j+1} - x_j)} \end{pmatrix} \cdot \begin{pmatrix} C_j \\ D_j \end{pmatrix} \\ &=: M_p(x_{j+1} - x_j) \cdot \begin{pmatrix} C_j \\ D_j \end{pmatrix}. \end{aligned} \tag{2.38}$$

The values of the electric fields in the array are fixed by the incoming beam amplitudes A_1 and D_N. The total reflection and transmission coefficients are calculated with the help of the total transfer matrix of the setup and define the remaining amplitudes at the boundaries as $B_1 = \mathfrak{r}_l^{tot} A_1 + \mathfrak{t}^{tot} D_N$ and $C_N = \mathfrak{r}_r^{tot} A_1 + \mathfrak{t}^{tot} D_N$ self-consistently.

Due to the fact that the product of transfer matrices are always of the form (2.32) we can define the group[1] of transfer matrices $(\mathcal{T}, \cdot)$, where $\cdot$ stands for the standard matrix-multiplication, and $\mathcal{T}$ is defined as follows [15]

$$\mathcal{T} := \left\{ T \in \mathbb{C}^{2\times 2} \middle| \exists\, \mathfrak{r}_l, \mathfrak{r}_r, \mathfrak{t} \in \mathbb{C} : T = \frac{1}{\mathfrak{t}} \begin{pmatrix} \mathfrak{t}^2 - \mathfrak{r}_l \mathfrak{r}_r & \mathfrak{r}_r \\ -\mathfrak{r}_l & 1 \end{pmatrix} \equiv T(\mathfrak{r}_l, \mathfrak{r}_r, \mathfrak{t}) \right\}. \tag{2.39}$$

In this case the coefficients $\mathfrak{r}_l$ and $\mathfrak{r}_r$ no longer have to be the same because for arrays of beam splitters reflection from left and right must not be equal [15].

[1] A group is a set G together with an operation $\cdot$, short written as $(G, \cdot)$ which fulfils the following conditions $(a, b, c \in G)$ [23]:

- Closure: $a, b \in G \to a \cdot b \in G$
- Associativity: $a \cdot (b \cdot c) = (a \cdot b) \cdot c$
- Existance of a neutral element: $\exists e \in G \to a \cdot e = e \cdot a = a$
- Existance of an inverse element: $\exists i \in G \to i \cdot b = b \cdot i = e$ $(i := b^{-1})$

It is easy to show that (2.39) fulfils all the group axioms. First we need to find out that $T_1 \cdot T_2 \in \mathcal{T}$ if $T_1, T_2 \in \mathcal{T}$. For that we define two matrices $T_1, T_2 \in \mathcal{T}$

$$T_1 = \frac{1}{\mathfrak{t}} \begin{pmatrix} \mathfrak{t}^2 - \mathfrak{r}_l \mathfrak{r}_r & \mathfrak{r}_r \\ -\mathfrak{r}_l & 1 \end{pmatrix}, \tag{2.40a}$$

$$T_2 = \frac{1}{\mathfrak{T}} \begin{pmatrix} \mathfrak{T}^2 - \mathfrak{R}_l \mathfrak{R}_r & \mathfrak{R}_r \\ -\mathfrak{R}_l & 1 \end{pmatrix}. \tag{2.40b}$$

Multiplying the matrices (2.40) results in

$$\begin{aligned} T^{\text{tot}} &= \frac{1}{\mathfrak{t}\mathfrak{T}} \begin{pmatrix} -\mathfrak{R}_l \mathfrak{r}_r + (-\mathfrak{r}_l \mathfrak{r}_r + \mathfrak{t}^2)(-\mathfrak{R}_l \mathfrak{R}_r + \mathfrak{T}^2) & \mathfrak{r}_r - \mathfrak{r}_l \mathfrak{r}_r \mathfrak{R}_r + \mathfrak{R}_r \mathfrak{t}^2 \\ -\mathfrak{R}_l + \mathfrak{r}_l \mathfrak{R}_l \mathfrak{R}_r - \mathfrak{r}_l \mathfrak{T}^2 & 1 - \mathfrak{r}_l \mathfrak{R}_r \end{pmatrix} \\ &=: \frac{1}{\mathfrak{t}^{\text{new}}} \begin{pmatrix} (\mathfrak{t}^{\text{new}})^2 - \mathfrak{r}_l^{\text{new}} \mathfrak{r}_r^{\text{new}} & \mathfrak{r}_r^{\text{new}} \\ -\mathfrak{r}_l^{\text{new}} & 1 \end{pmatrix} \end{aligned} \tag{2.41}$$

where we defined

$$\mathfrak{t}^{\text{new}} = \frac{\mathfrak{t}\mathfrak{T}}{1 - \mathfrak{r}_l \mathfrak{R}_r}, \tag{2.42a}$$

$$\mathfrak{r}_l^{\text{new}} = (\mathfrak{R}_l - \mathfrak{r}_l \mathfrak{R}_l \mathfrak{R}_r + \mathfrak{r}_l \mathfrak{T}^2) \mathfrak{t}^{\text{new}}, \tag{2.42b}$$

$$\mathfrak{r}_r^{\text{new}} = (\mathfrak{r}_r - \mathfrak{r}_l \mathfrak{r}_r \mathfrak{R}_r + \mathfrak{R}_r \mathfrak{t}^2) \mathfrak{t}^{\text{new}}. \tag{2.42c}$$

To check if T^{tot} is an element of $\mathcal{T}$ we calculate the entry T_{11}^{tot} with (2.42) and check if this fullfills the following equation

$$\frac{(\mathfrak{t}^{\text{new}})^2 - \mathfrak{r}_l^{\text{new}} \mathfrak{r}_r^{\text{new}}}{\mathfrak{t}^{\text{new}}} = \frac{-\mathfrak{R}_l \mathfrak{r}_r + (-\mathfrak{r}_l \mathfrak{r}_r + \mathfrak{t}^2)(-\mathfrak{R}_l \mathfrak{R}_r + \mathfrak{T}^2)}{\mathfrak{t}\mathfrak{T}}. \tag{2.43}$$

Due to the fact that this is the case and also knowing that all matrices out of $\mathcal{T}$ have determinant 1, meaning they are invertible, i.e. there exists an inverse element, we are able to state that $(\mathcal{T}, \cdot)$ is a group (The neutral element is trivial in this case because it corresponds to the unity matrix). In addition, one should notice that the transfer matrices have a reflection symmetry where $\sigma_z T \sigma_z = T^{-1}$ and $\sigma_z = \left(\begin{smallmatrix} 0 & 1 \\ 1 & 0 \end{smallmatrix}\right)$ is the Pauli Matrix for the z direction.

We are now able to calculate several fields for an array of beam splitters just by matrix multiplication. The calculation of the forces on polarizable particles is straight forward as shown in the following chapter.

2.3.2 Force onto a single beam splitter

Using the Maxwell stress tensor (2.12) we are able to calculate the force on every single beam splitter with equation (2.14). Due to the fact that the beam splitter method is a

one dimensional method we can simplify (2.12) to

$$\begin{aligned} T_{xx} &= \epsilon_0 \left[E_x E_x + c^2 B_x B_x - \frac{1}{2}(E_x^2 + E_y^2 + E_z^2 + c^2[B_x^2 + B_y^2 + B_z^2]) \right] \\ &= -\frac{\epsilon_0}{2} \left(\mathbf{E}^2 + c^2 \mathbf{B}^2 \right), \end{aligned} \tag{2.44}$$

where we used the fact that the electric and magnetic fields are always orthogonal to the propagation direction resulting in $E_x = B_x = 0$ (assuming field propagation in x direction). Another simplification of equation (2.44) can be achieved by using the fact that electromagnetic waves are transversal, i.e. $|c\mathbf{B}| = |\mathbf{E}|$, resulting in

$$T_{xx} = \epsilon_0 \mathbf{E}^2. \tag{2.45}$$

In the case of infinitesimally thin beam splitters we are dealing with, the integration volume is given via $V = \mathcal{A}/2\ \delta l$, where δl corresponds to an infinitesimally small length parallel to the x-axis. This length has no influence on the integral in (2.14). The two surfaces with size $\mathcal{A}/2$ are chosen parallel to the beam splitter, which is localized at position $x = x_j$. Therefore the vector $\mathbf{n}$ is defined as $\mathbf{n} = \mathcal{A}/2\ \mathrm{sign}(x - x_j)\mathbf{e}_x$. Under these assumptions the integral (2.14) can be calculated through

$$F_\alpha = \frac{\mathcal{A}}{2} \left[-T_{xx}(x \to x_j^-) + T_{xx}(x \to x_j^+) \right]. \tag{2.46}$$

Using Maxwell's stress tensor (2.45) together with the fields (2.29) yields the time averaged force per unit area on the jth beam splitter as [13]

$$\mathcal{F}_j = \frac{\epsilon_0}{2} \left[|A_j|^2 + |B_j|^2 - |C_j|^2 - |D_j|^2 \right]. \tag{2.47}$$

This simple but powerful formalism to calculate the fields and forces on single atoms, atom clouds or other dielectric media such as membranes or elastic dielectrics allows us to describe complex dynamics such as self–organization or even laser cooling in any effective 1D geometry [21, 24–26].

2.3.3 Generalization for multiple frequencies and polarizations

Previous models were restricted to a single pump frequency and polarization in a counter propagating geometry. Here we show that it is straightforward to generalize the beam splitter method to allow for multiple frequencies and polarizations. The field propagating in the x-direction shall then be written as $\mathbf{E}(x,t) = E_y(x)\exp(-i\omega_y t)\mathbf{e}_y + E_z(x)\exp(-i\omega_z t)\mathbf{e}_z$, where $E_y(x)$ $[E_z(x)]$ is defined as the component polarized in the direction of $\mathbf{e}_y$ $[\mathbf{e}_z]$ oscillating with frequency $\omega_y = k_y c$ $[\omega_z = k_z c]$. In this setup, the beam splitter model can be employed for each component independently, as long as the particles don't scatter photons from one mode into the other. Here we wrote that

the total field is a sum of linearly polarized fields, but using two orthogonal circular polarizations would not change the main conclusions.

Note that the coupling parameter ζ introduced in equation (2.6) is proportional to the atomic polarizability and the wave vector. In this thesis we will assume that the polarizability is the same for k_y and k_z, hence $\zeta_z = \zeta_y k_z/k_y$. Of course, a more realistic treatment of α is easily possible within our framework but it would add unnecessary complexity.

In the following chapters we will study how the introduction of different frequency fields provides new prospects of manipulating arrays of particles, ranging from equidistant lattices to individually tuned inter-particle distances as well as the design and control of motional couplings.

Chapter 3

Possible realization methods

Before continuing with the model calculations considered in this thesis we would like to give a short overview of possible experimental realisations which have been developed recently. Even though the beam splitter method is a one dimensional method there are some experimental configurations which fulfil several conditions for being described within this method.

The main condition which has to be fulfilled is that the particles have only one effective degree of freedom meaning the interesting dynamics occurs along one axis. If this condition holds other three dimensional effects such as scattering losses in all three dimensions can be included into the imaginary part of the parameter ζ.

Originally, the beam splitter method was developed to describe atoms in 1D optical lattices [12, 13]. In recent years new experimental setups with effective 1D geometry have been developed, which can perfectly be described by the beam splitter method. In this chapter we will give a short description of two of these 1D geometries which could reproduce the results discussed in this thesis. In addition, we will show how the parameter ζ, which describes the scattering properties of each particle can be estimated for special experimental setups.

3.1 Atoms trapped in the evanescent field surrounding an optical nanofibre

The first approach was developed by Rauschenbeutel and co-workers a few years ago [4]. They established a method to trap caesium atoms alongside a tapered nanofibre. The diameter of this fibre (usually 500 nm) is smaller than the wavelength of the incoupled laser (1064 nm) resulting in an high evanescent field outside the fibre. Generally they realize a two-colour optical dipole trap. This fibre-based atom trap is a quasi 1D geometry meaning that it can be well described with the beam splitter method. The experimental setup is shown in figure 3.1a.

The red-detuned light field attracts the atoms towards the nanofibre while the blue-

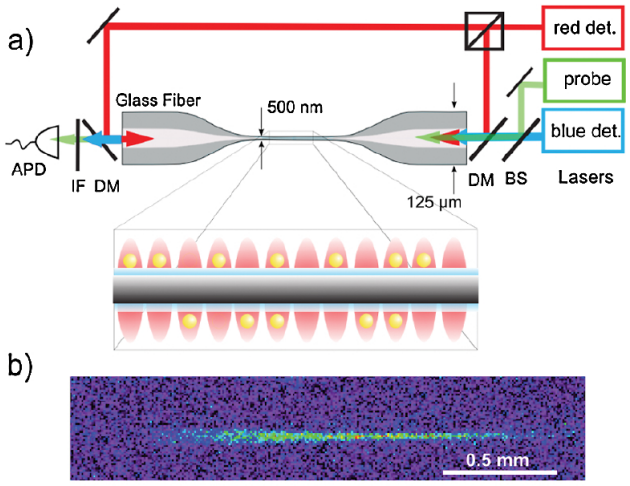

Figure 3.1: (a) Experimental setup to generate an atom-trap alongside a tapered nanofibre. The trapping potential is generated as a combination of a blue- and a red-detuned laser fields. (b) Fluorescence image of the trapped atomic ensemble. (source: [4]).

detuned field repels them from the fibre. The radial dependencies of these two potentials are different (cf. figure 3.2a), resulting in a net potential minimum a few hundred nanometres from the nanofibre surface. To confine the atoms in axial directions the red detuned laser is imposed from both sides, resulting in a standing wave potential. Azimuthal confinement is due to the fact that the used HE_{11} is azimuthally dependent. These confinements result in atom traps on both sides along the nanofibre cf. figure 3.2d. Related setups by other groups have also been established in the last few years [9].

As we believe that this trap configuration could also be used to verify the systems we are considering in the following chapters, we would like to give a short argumentation why all the conditions for being treated with the beam splitter method are fulfilled.

Due to the fact that every atom trapped at the surface of the fibre can interact with the fibre mode via the evanescent field it has the same scattering properties as a beam splitter. It can absorb photons from the fibre mode and emit them back into the fibre mode. The scattering loss due to spontaneous emission corresponds to the imaginary part of ζ.

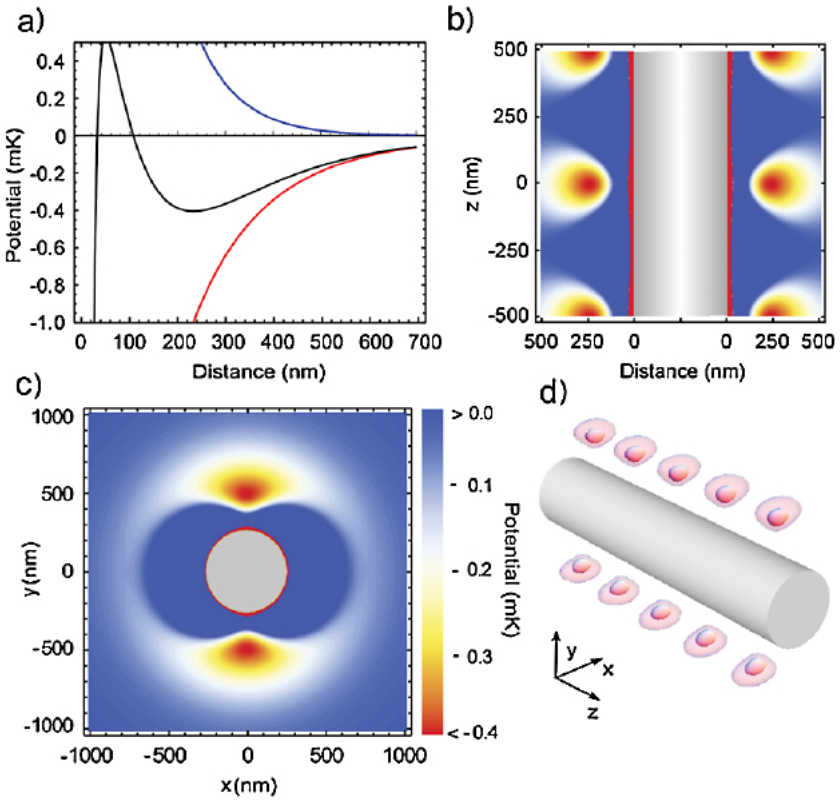

Figure 3.2: Potential generated for atoms along a tapered nano fibre. (a) Radial dependencies as a function of distance from the nanofibre. The red-detuned light field results in an attractive potential (red curves) while the blue-detuned light field generates a repelling force (blue curves). Due to the different radial dependence the resulting potential has a minimum a few hundred nanometres outside the fibre (black curve). (b) Contour plot of the potential. Axial confinement is obtained by a standing wave trap. (c) Azimuthal dependence of the potential, (d) schematic view of the generated array of trapping sites. (source: [4]).

3.2 Nanospheres in a hollow core fibre

A second approach uses classical objects, namely nanospheres. Aspelmeyer and co-workers established a method to trap and manipulate nanospheres inside the core of a hollow core fibre [27].

These fibres are hollow nanofibres surrounded by an photonic band gap material which ensures maximal light propagation inside the fibre. In figure 3.3 a lateral-cut of such a fibre is shown.

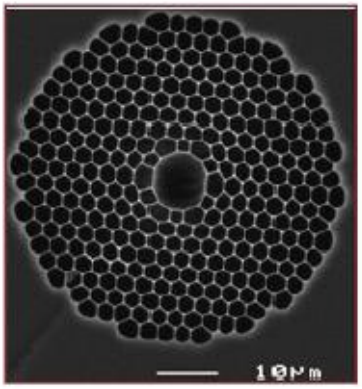

Figure 3.3: Lateral-cut of a hollow core fibre by NKT Photonics (source: [27]).

The nanospheres used in this experiment have a radius of 127 nm, i.e. they are much smaller than the wavelength of the laser light (1064 nm). This allows us to describe the particles as single dipoles which scatter light back into the fibre mode (i.e. the geometry must not be taken into account). Of course this setup can be very well treated with the beam splitter method meaning that every nanosphere is modelled as a beam splitter, which scatters light back into the fibre mode. Scattering losses and heating of the spheres due to absorption can be included to the imaginary part of ζ.

3.3 Estimation of the parameter ζ

As far as experimental setups are concerned it is crucial to know the parameter ζ, as defined in section 2.3, for the specific particles used in the experiment. In this chapter it is shown how this parameter can be evaluated out of the measured reflection and transmission of the particle.

In equation (2.36) the dependence of the complex reflection and transmission coefficient $\mathfrak{r}$ and $\mathfrak{t}$ on the parameter ζ is given. The measurable quantities in this case are $R := |\mathfrak{r}|^2$ and $T := |\mathfrak{t}|^2$ which can be written in terms of the real- and imaginary part of

the parameter ζ

$$R = \frac{\mathrm{Re}^2(\zeta) + \mathrm{Im}^2(\zeta)}{1 + 2\,\mathrm{Im}(\zeta) + \mathrm{Im}^2\,\zeta + \mathrm{Re}^2(\zeta)}, \tag{3.1a}$$

$$T = \frac{1}{1 + 2\,\mathrm{Im}(\zeta) + \mathrm{Im}^2\,\zeta + \mathrm{Re}^2(\zeta)}. \tag{3.1b}$$

Equations (3.1) defines a system which can be solved for $\mathrm{Re}(\zeta)$ and $\mathrm{Im}(\zeta)$ resulting in

$$\mathrm{Re}(\zeta) = \pm\frac{\sqrt{(1+R+T)^2 - 2(1+R^2+T^2)}}{2T}, \tag{3.2a}$$

$$\mathrm{Im}(\zeta) = \frac{1-R-T}{2T}. \tag{3.2b}$$

The sign of the real part of ζ depends on the properties of the used particles, i.e. whether they are high-field seekers or low-field seekers, cf. equation (2.28b). In summary, the real and imaginary part of ζ can be easily estimated by measuring the reflected and transmitted light of a single particle.

Chapter 4

Light forces in counter propagating beams with orthogonal polarization

In this chapter we explore forces and dynamics of a 1D array of scatterers modelled by a chain of beam splitters at distances $d_j := x_{j+1} - x_j$ irradiated from both sides by light with orthogonal polarizations ($\mathbf{e}_y$ and $\mathbf{e}_z$) and possibly distinct frequencies (ω_y and ω_z), cf. figure 4.1. In contrast to a standard optical lattice setup as treated in previous publications [12, 13] no a priori intensity modulation due to wave interference is present and we start with a translation invariant field configuration.

Hence the light field itself does not prescribe any a priori local ordering and only multiple light scattering from the particles themselves creates spatially varying trapping forces. Due to the translation invariance of the setup no absolutely stable particle configuration can be expected. However, the coupled particle field dynamics can induce relative order. Hence our central goal is to find conditions, when the light forces induced by two non-interfering beams are sufficient to obtain stationary stable particle arrays, and analyse how this spontaneous crystal formation arises.

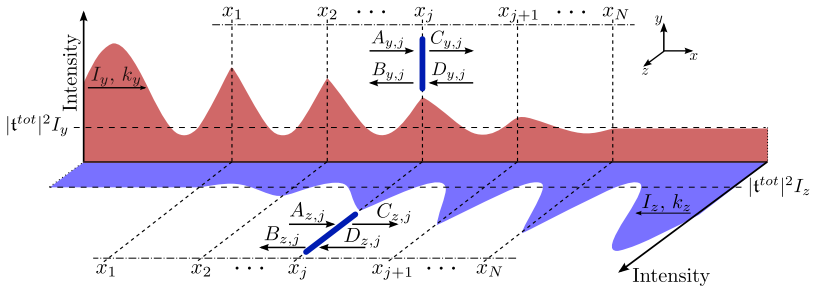

Figure 4.1: Sketch of the intensity distribution of two light fields of orthogonal polarization and different colour propagating through a 1D array of thin beam splitters. Light with orthogonal polarization is imposed from left and right.

4.1 Stability conditions for two beam splitters

To get some first insight, we start with the simplest non-trivial example of two beam splitters at a distance $d = x_2 - x_1$. The pump intensities from the left and right beam are given as $I_y = \frac{c\varepsilon_0}{2}|A_{y,1}|^2$ and $I_z = \frac{c\varepsilon_0}{2}|D_{z,2}|^2$, respectively. Here we choose the convention that all variables with index y corresponding to light polarized in direction of $\mathbf{e}_y$, which is injected from the left (negative x-axis), and index z corresponding to $\mathbf{e}_z$-polarized light injected from the right. The individual beam splitters are counted from left to right with integer indices, so that $B_{z,2}$ is the B-amplitude of the light field polarized parallel to $\mathbf{e}_z$ at the second beam splitter, cf. equation (2.27).

We also have to keep in mind that the coupling parameter $\zeta = k\eta\alpha/(2\varepsilon_0)$ explicitly depends on the wave numbers k_y and k_z. We will assume that the atomic polarizability α is frequency independent, i.e. the same for both frequencies used and hence the effective interaction parameters are defined as $\zeta_z \equiv \frac{k_z}{k_y}\zeta$, $\zeta_y \equiv \zeta$.

To calculate the forces on each beam splitter of this system one first has to know all the amplitudes to use (2.47) which can be easily achieved via transfer matrix multiplication. Figure 4.2 shows all amplitudes which have to be considered in this system.

We will not list the detailed calculation, but just shortly give an idea how the mechanism works. The following linear equation can be solved for $B_{y,1}$ and $C_{y,2}$

$$(A_{y,1}, B_{y,1})^T = (M_{BS})^{-1} \cdot (M_p(d))^{-1} \cdot (M_{BS})^{-1} \cdot (C_{y,2}, 0)^T. \tag{4.1}$$

With this result one can calculate $(A_{y,2}, B_{y,2})^T = (M_{BS})^{-1} \cdot (C_{y,2}, 0)^T$. Now using equation (2.47) results in the force $\mathcal{F}_{y,2}$ induced by light with wave number k_y and polarization along $\mathbf{e}_y$ onto the second beam splitter. We use light with different polarizations and as discussed in section 2.3.3 the corresponding forces can be calculated separately and added to obtain the total force on both beam splitters. Proceeding with $(C_{y,1}, D_{y,1})^T = (M_p)^{-1} \cdot (A_{y,2}, B_{y,2})^T$ and using equation (2.47) again, leads us to the

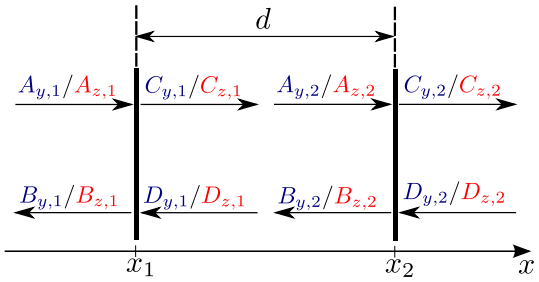

Figure 4.2: System of two beam splitters. The amplitude's first index stands for the wavelength, the second corresponds to the beam splitter number. $A_{y,1}$ and $D_{z,2}$ are proportional to the incoming intensities from each side. In our system the amplitudes $D_{y,2}$ and $B_{z,1}$ will always be zero, because only two light sources with different polarizations and wavelengths on the left and right side are considered.

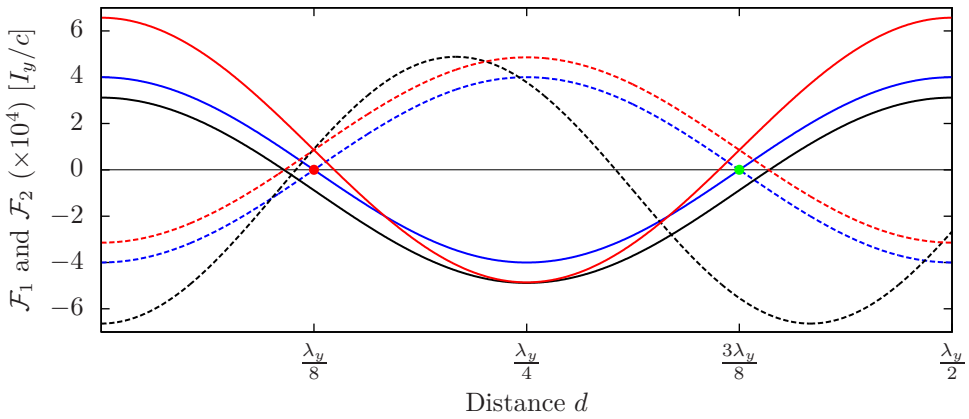

Figure 4.3: Force on left (4.2a) (solid lines) and right beam splitter (4.2b) (dashed lines) as function of distance d in units of I_y/c for $\zeta = 0.01$ and $k = k_y = k_z = 2\pi/\lambda$. For equal pump power $\mathcal{P} = I_z/I_y = 1$ and frequency (blue curves) two the forces add to zero and vanish at distances $d = \lambda/8$ and $d = 3\lambda/8$. For asymmetric pump intensities $\mathcal{P} = 0.7$ (red curves) a net centre of mass force remains. The black curve shows a similar behaviour occurring for different pump frequencies $\frac{k_z}{k_y} = 1.2$ of the same power $\mathcal{P} = 1$. The red (green) dot marks unstable (stable) stationary points.

force $\mathcal{F}_{y,1}$. Analogous to the previous calculations one can also find the forces $F_{z,1}$ and $F_{z,2}$ induced by light with wave number k_z and polarized along $\mathbf{e}_z$. The only thing one has to take care of is that for different wavelengths the parameter ζ changes. In the following, we will assume the same polarizability for both wavelengths which means that for the second wavelength, ζ has to be replaced by $\zeta_2 \equiv \frac{k_2}{k_1}\zeta$ in the transfer matrices. The total forces can then be found via $\mathcal{F}_1 = \mathcal{F}_{y,1} + \mathcal{F}_{z,1}$ and $\mathcal{F}_2 = F_{y,2} + \mathcal{F}_{z,2}$.

Despite the simple physical situation the corresponding general analytic solution already is rather unhandy. Thus we first restrict ourselves to real valued ζ neglecting absorption in the beam splitter or equivalently neglecting spontaneous emission in an atom fibre system. Assuming small values of ζ and dropping terms of $\mathcal{O}(\zeta^3)$ and higher, we then find the following approximate formulae for the force on the two particles

$$\mathcal{F}_1 = \frac{1}{c}\left(\frac{I_y\, 2\zeta^2\,(4\cos^2(dk_y) - 1)}{1 + 4\zeta^2\cos^2(dk_y)} - \frac{I_z\, 2(\frac{k_z}{k_y}\zeta)^2}{1 + 4(\frac{k_z}{k_y}\zeta)^2\cos^2(dk_z)}\right), \tag{4.2a}$$

$$\mathcal{F}_2 = \frac{1}{c}\left(\frac{I_y\, 2\zeta^2}{1 + 4\zeta^2\cos^2(dk_y)} - \frac{I_z\, 2(\frac{k_z}{k_y}\zeta)^2\,(4\cos^2(dk_z) - 1)}{1 + 4(\frac{k_z}{k_y}\zeta)^2\cos^2(dk_z)}\right). \tag{4.2b}$$

For a given set of control parameters, namely the pump power ratio $\mathcal{P} := I_z/I_y$ and the wave numbers k_y and k_z, the beam splitters will settle at a distance d_0 for which the two forces are equal i.e. $\mathcal{F}_1|_{d=d_0} = \mathcal{F}_2|_{d=d_0}$ and the configuration is stable $\partial_d\mathcal{F}_1|_{d=d_0} > 0$ and $\partial_d\mathcal{F}_2|_{d=d_0} < 0$. In this case, the system can still exhibit centre of mass motion but

the particles are fixed at a constant distance. From equation (4.2) we see that a stable configuration in the special case of equal wave numbers, $k = k_y = k_z$ requires

$$\Delta\mathcal{F} = \mathcal{F}_1 - \mathcal{F}_2 = \frac{1}{c}\frac{4\zeta^2\cos(2d_0k)}{1+4\zeta^2\cos^2(d_0k))}\left(I_y + I_z\right) = 0. \tag{4.3}$$

Independent of the injected laser intensities, which just appear as a multiplicative factor, this corresponds to two particles at distance $d_0^s = \frac{(2n+1)\pi}{4k} = \frac{(2n+1)\lambda}{8}$ ($n \in \mathbb{N}$) cf. figure 4.3. Here the solutions for odd n correspond to a stable configuration, while even n leads to unstable behaviour. As numerical example we plot the full distance dependent forces for three typical sets of parameters in figure 4.3, where stationary distances of equal force can be read of the intersection points. If these occur at zero force, the centre of mass is stationary as well.

4.1.1 Stability analysis as a function of distance

The centre of mass is stationary if the total force, i.e. the sum of both forces (4.2), vanishes. To find out whether there are some special distances d for which the system is stable when light with different polarizations is used, we search for the zeros of equations (4.2). We assume $k_1 = k_2 \equiv k$ in (4.2).

For small ζ the distances of zero force on each particle can be approximated by

$$d_1^{\pm} = \frac{1}{k_y}\left[\arccos\left(\pm\frac{1}{2k_y}\sqrt{\frac{k_y^2I_y + k_z^2I_z}{I_y + (k_z/k_y)^2\zeta^2\left(I_y - I_z\right)}}\right) + n_1\pi\right] \qquad n_1 \in \mathbb{Z}, \tag{4.4a}$$

$$d_2^{\pm} = \frac{1}{k_z}\left[\arccos\left(\pm\frac{1}{2k_z}\sqrt{\frac{k_y^2I_y + k_z^2I_z}{I_z - \zeta^2\left(I_y - I_z\right)}}\right) + n_2\pi\right] \qquad n_2 \in \mathbb{Z}. \tag{4.4b}$$

Conditions (4.4) imply $\mathcal{F}_1|_{d=d_1^{\pm}} = 0$ and $\mathcal{F}_2|_{d=d_2^{\pm}} = 0$, respectively. Any solution fulfilling $d_1^- = d_2^-$ thus results in a stable and stationary configuration, where the forces on both beam splitters vanish and small perturbations induce a restoring force, as cf. figure 4.3. Such solutions can only be determined numerically and are not guaranteed to exist for any set of parameters.

4.1.2 Stability analysis as a function of intensities

In section 4.1.1 we saw that distances with vanishing force on both beam splitters, leading to a stable or trapped configuration for given pump-power ratios and wave numbers for the special case $k = k_y = k_z$ require equal pump power. If we reverse the line of argumentation and ask for pump-power ratios and wave numbers where the two beam splitters can be trapped at a given distance d, the result allows us to study the full system i.e. different polarizations *and* frequencies. In this case precise distance control is possible.

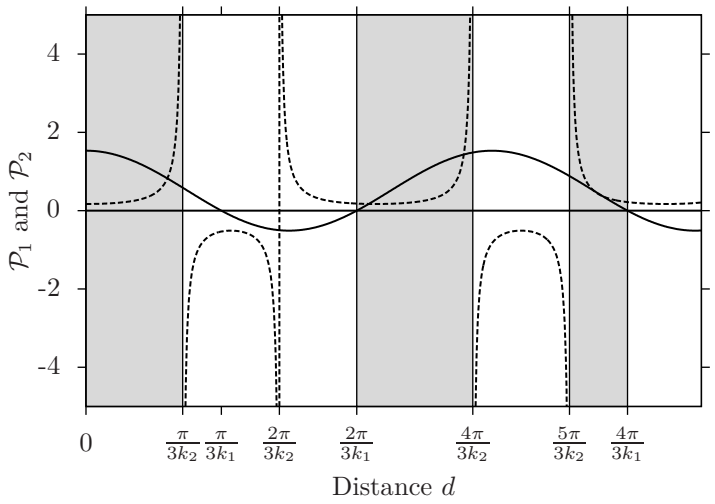

Figure 4.4: Pump-power ratio leading to stable solutions (4.5a) (solid line) and (4.5b) (dashed line) for a prescribed distance d for $\zeta = 0.01$ and $k_z/k_y = 1.4$. The grey regions mark regions where the physically allowed regions $\mathcal{P}_1 > 0$ and $\mathcal{P}_2 > 0$.

First we need to find the zeros of (4.2) with respect to $\mathcal{P}$:

$$\mathcal{P}_1 = \frac{(4\cos^2(dk_y) - 1)(k_y^2 + 4k_z^2\,\zeta^2\cos^2(dk_z))}{k_z^2\,(1 + 4\zeta^2\cos^2(dk_y))} \tag{4.5a}$$

$$\mathcal{P}_2 = \frac{k_y^2 + 4k_z^2\,\zeta^2\cos^2(dk_z)}{k_z^2\,(1 + 4\zeta^2\cos^2(dk_y))(4\cos^2(dk_z) - 1)}. \tag{4.5b}$$

Both solutions $\mathcal{P}_1$ and $\mathcal{P}_2$ have to be positive, which is not valid for all values of d (cf. figure 4.4). The denominator diverges for $d = \frac{n\pi}{3k_2}$, with $n \in \{1, 2, 4, 5, 7, ...\}$ (all multiples of 3 are neglected for n). In addition, both, $\mathcal{P}_1$ and $\mathcal{P}_2$, have to be positive for physical reasons. Figure 4.4 shows the functional dependence of the solutions (4.5a) and (4.5b) on the distance d. Due to the condition that both solutions have to be positive, not all distances lead to a physical solution. If $k_2 > k_1$, just distances in the intervals $(0, \frac{\pi}{3k_2})$, $(\frac{2\pi}{3k_2}, \frac{4\pi}{3k_2})$ and so on are allowed as can be seen in figure 4.4. In the case where $k_2 < k_1$, the intervals remain the same, but k_2 has to be replaced by k_1.

To obtain a trapping condition for the wave numbers i.e. wave numbers where the total force $\mathcal{F}_1 + \mathcal{F}_2$ vanishes, we solve $\mathcal{P}_1 = \mathcal{P}_2$, finding

$$k_z^{\pm} = \frac{1}{d}\arccos\left(\pm\frac{\sqrt{\cos(2dk_y)}}{\sqrt{2(1 + 2\cos(2dk_y)}}\right) + 2\pi n, \qquad n \in \mathbb{Z}. \tag{4.6}$$

Equation (4.6) enables us to calculate the needed wave numbers, to trap the beam splitters at a given distance d. The associated pump-power ratio can be calculated via (4.5a) or (4.5b).

Of course one can also can ask for a self-organized system in this context. Again we calculate $F_1 - F_2 = 0$ for $\mathcal{P}$ and get

$$\mathcal{P} = -\frac{(2\cos(dk_1)^2 - 1)(k_1^2 + 4k_2^2\zeta^2\cos(dk_2)^2)}{k_2^2(1 + 4\zeta^2\cos(dk_1)^2)(2\cos(dk_2)^2 - 1)}. \tag{4.7}$$

We notice that for $k_1 = k_2 \equiv k$ the pump-power ratio (4.7) simplifies to $\mathcal{P} = -1$. This does not fulfil the condition that $\mathcal{P}$ has to be positive, meaning that for any given distance d there is no possibility to imply a centre of mass motion in the case that $k_1 = k_2 \equiv k$.

In principle, determining stationary states for a larger number of beam splitters is straightforward by first solving equations (2.37) and (2.38) for the fields and using these to calculate the forces. However, to determine a completely stationary configuration of N splitters for a given input field configuration, we have to solve N non-linear equations to guarantee a vanishing force at each beam splitter as function of the $N - 1$ relative distances. This problem can have no or infinite many solutions. Often one does not get an exact solution, but solutions with vanishingly small centre of mass force.

As a rather tractable example we plot the zero force lines as function of the two relative distances for the case of three beam splitters illuminated by light of equal power, $\mathcal{P} = 1$, but different colour, $k_z/k_y = 1.1$ in figure 4.5. One finds many intersections of these lines, where two forces vanish, but only for a few distances we get triple intersections where the forces on all three mirrors vanish and stationary order can be achieved. These solutions then still have to be checked for stability against small perturbations to find a stable steady state.

In general we see that despite the lack of externally prescribed order the particles mostly tend to arrange a configuration with stationary distance. While finding explicit analytical formulas here is rather tedious, a numerical evaluation requires very little effort and can be easily performed for large parameter ranges. This will be done in the following section.

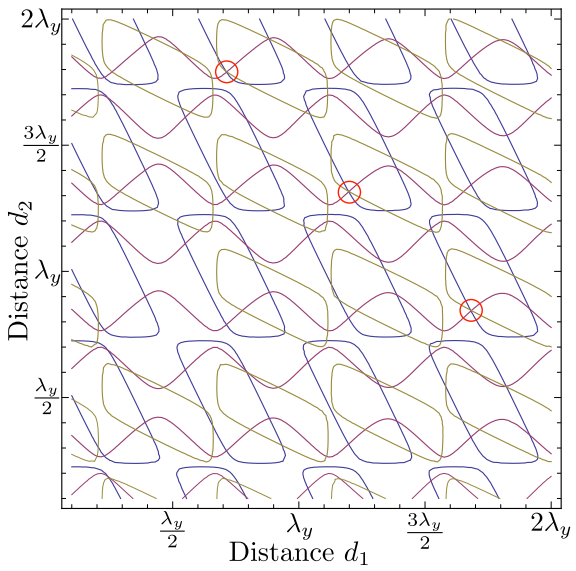

Figure 4.5: Zero force lines for three beam splitters as function of the two distances for $k_z/k_y = 1.1$, $\zeta = 0.1$ and equal power $\mathcal{P} = 1$. Common crossings of all three lines (red circles) denote a stationary (but possibly unstable) configuration with no centre of mass motion.

4.2 Self-ordering dynamics

To investigate the dynamics of a higher number of beam splitters even the numerical solution for stationary states from the force equations gets more and more tedious. Hence it is more instructive to change into the time domain picture and solve the dynamical Newtonian equations of motion (4.9) for various initial conditions until an equilibrium configuration is reached. To arrive at a stationary solution we assign a mass to the beam splitters and add an effective friction term with friction coefficient μ to the classical Newtonian equations of motion [13],

$$m\ddot{x}_j = -\mu\dot{x}_j + F_j(x_1, ..., x_N). \tag{4.8}$$

In the following simulations we assume that the system is in the so called over-damped regime, meaning that the characteristic time scale of undamped cloud motion, i.e. the oscillation period, is much larger than the relaxation time of the cloud's velocity towards a constant value due to viscous friction. Under this assumption the equations of motion (4.8) are reduced to a set of differential equations of first order [13],

$$\dot{x}_j = \frac{F_j(x_1, ..., x_N)}{\mu}. \tag{4.9}$$

First we would like to check if the analytical result (4.4a) which was obtained from a static approach, can be reproduced in this dynamical picture. For that purpose

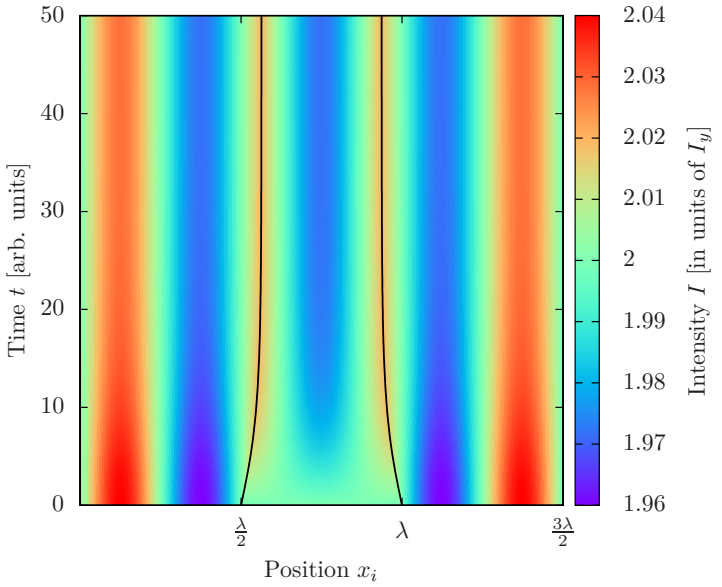

Figure 4.6: Dynamics for $N = 2$ beam splitters, using $\mathcal{P} = 1$, $k_y = k_z$ and $\zeta = 0.01$ starting at initial distance $\lambda/2$. The colour coding in the background shows the corresponding evolution of the total field intensity $I_{tot} := I_y + I_z$.

we simulate the dynamics of two beam splitters in the symmetric case ($\mathcal{P} = 1$ and $k_z/k_y = 1$) with equation (4.9).

In a traditional standing wave trap, the beam splitters would settle at the chosen initial equidistant spacing $d_{init} = \pi/k = \lambda/2$, cf. equation (5.19), which can be determined self-consistently [13]. However, for two trap beams of orthogonal polarization no prescribed periodicity is present and the particles themselves create a field configuration which confines their motion through multiple scattering.

For two particles we find that they rearrange from their starting distance point towards a smaller distance. They settle again at a stable configuration where the resulting distance is close to the estimated one in the static case $d_a = 3\lambda/8$ cf. figure 4.6 and figure 4.7. The small difference between the analytical and numerical result in figure 4.7 results from neglecting orders $\mathcal{O}(\zeta^3)$ in (4.2a) and (4.2b).

Another fundamental question is what influence the imaginary part of ζ takes considering the stability of the system. In the analytical calculations performed in the previous chapters we assumed $\zeta \in \mathbb{R}$. In the numerical case it is easy to estimate how long this assumption is true. For that purpose we plot the dependence of the obtained stable distance between the two beam splitters on the imaginary part of ζ for fixed values of $\mathrm{Re}(\zeta)$, cf. figure 4.8.

Obviously the system is stable if the imaginary part of ζ is sufficiently small but in all cases we find that there exists a threshold for the imaginary part of ζ. Above

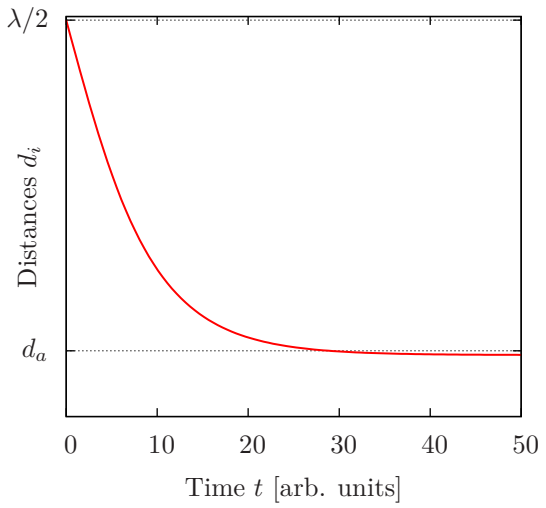

Figure 4.7: Comparison of the dynamically obtained distance $d := x_2 - x_1$ (red line) to the analytic result d_a given in equation (4.4a) (dashed line). The same parameters as in figure 4.6 are used.

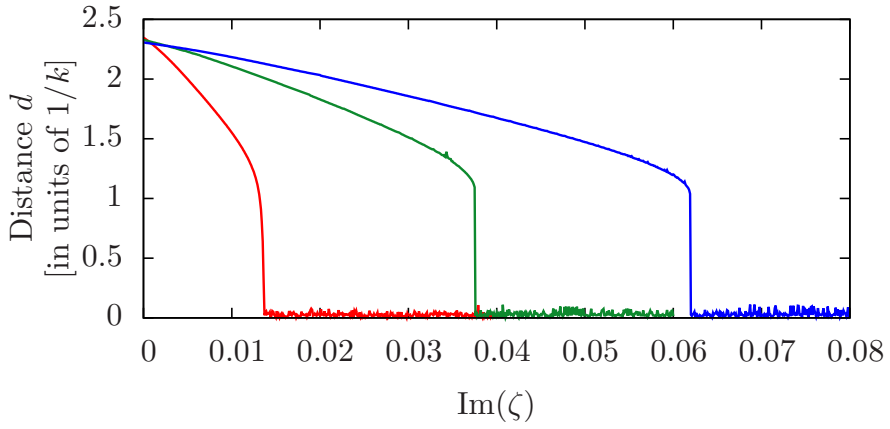

Figure 4.8: Distance between two beam splitters ($\mathcal{P} = 1$, $k = k_y = k_z$) as a function of $\mathrm{Im}(\zeta)$. The different curves correspond to different values of $\mathrm{Re}(\zeta)$: red curve $\mathrm{Re}(\zeta) = 0.01$, green curve $\mathrm{Re}(\zeta) = 0.03$, blue curve $\mathrm{Re}(\zeta) = 0.05$.

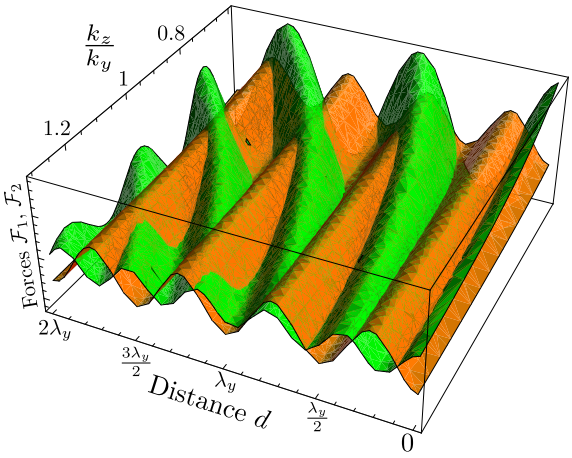

Figure 4.9: Force on left (orange) and right beam splitter (green) as function of the wave number ratio k_z/k_y and distance for two partly absorbing beam splitters with $\zeta = 1/12 - i/150$ and $\mathcal{P} = 1$.

this threshold the two particles are pushed together and no stable configurations with non-zero distance can be realized. This enables us to conclude that as long as the imaginary part of ζ remains smaller than the real part of ζ the system is stable and the expected effects should be the same. In the following we will mainly focus on real ζ to reduce the number of free parameters.

Let us now exhibit some more of the intrinsic complexity of the system in a numerical example. In figure 4.9 we plot the forces on the two beam splitters as function of distance and relative wave number for fixed equal pump intensity from both sides. Clearly the intersection of the two force surfaces shows a complex pattern with a multitude of stationary distances which can be controlled e.g. via the chosen frequency ratio.

In an alternative approach we can numerically find a stable stationary distance of the two beam splitters as function of pump power and wave number ratio by time integration of their motion with some damping added, cf. figure 4.10. We see that depending on the parameters for a given initial condition the system can settle to a large range of different stationary distances, exhibiting rather abrupt jumps at certain critical parameter values.

Generally a numerical evaluation requires very little effort and can easily be performed for large parameter ranges. This allows us to consider higher numbers of beam splitters as it is done in figure 4.11 with $N = 10$ beam splitters, we find that there are also stable and trapped solutions. Despite the fact that there is no externally prescribed order, the particles mostly tend to arrange at configurations with stationary distance, which differs from the one realized by a traditional standing wave, cf. figure 4.12.

We also find that in the special case where $k_z/k_y = 1$ $\mathcal{P} = 1$ is the only choice to obtain equally spaced beam splitters that are stable *and* trapped. This agrees with the analytical results for two beam splitters (4.4a). Interestingly, the final distances

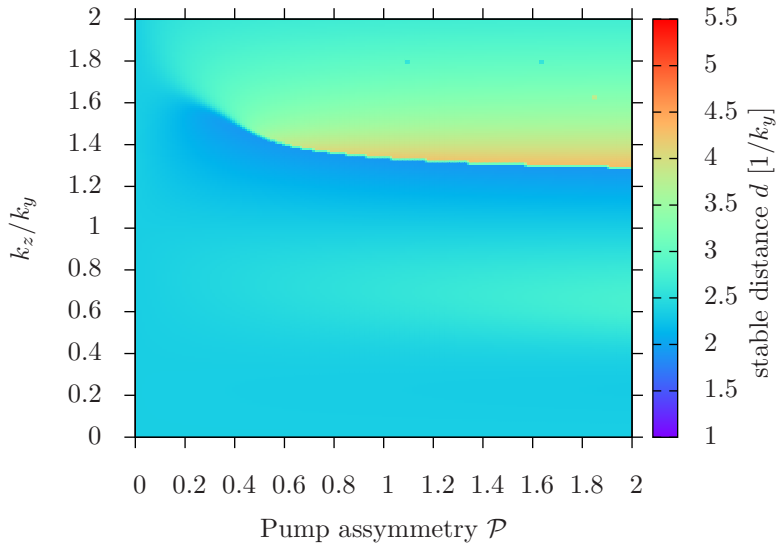

Figure 4.10: Stationary distance of two beam splitters with $\zeta = 0.01$ as function of the wave number ratio k_z/k_y and the pump power ratio $\mathcal{P}$ obtained by numerical integration of their equation of motion including an effective friction term.

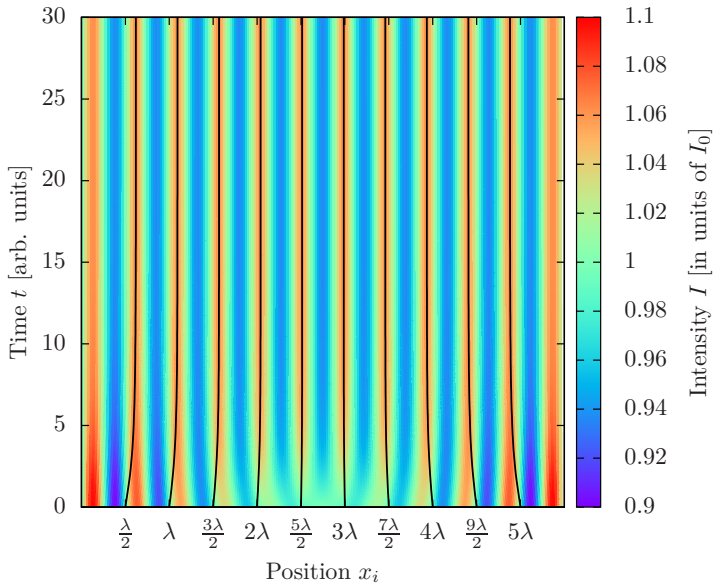

Figure 4.11: Trajectories of $N = 10$ beam splitters for $\mathcal{P} = 1$, $k_y = k_z$ and $\zeta = 0.01$ started from a regular array of distance $\lambda/2$. The colour coding in the background shows the corresponding evolution of the total field intensity $I_{tot} := I_y + I_z$.

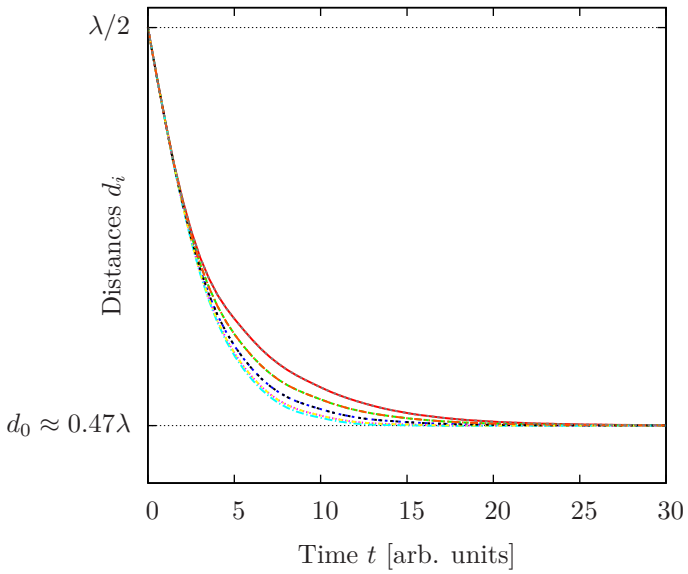

Figure 4.12: Change of the relative distances $d_i := x_{i+1} - x_i$ for the same parameters as in figure 4.11. Obviously they converge towards a stable equidistant order of reduced distance.

$d_1 = d_2 = ... = d_N$ converge to the result of the standing wave case as the number of beam splitters N is increased, cf. figure 4.13. In this case, a setup with orthogonally polarized trap beams has the same trapping properties as a standing wave setup, as $N \to \infty$. The beam splitters themselves form an effective Bragg reflector to synthesize a standing wave configuration, which then traps the particles.

A substantially more complex behaviour is found for the case of two colour illumination with different intensities, $I_y \neq I_z$. The trajectories for some representative cases can be found in figure 4.14. Interestingly, there is still a wide range of parameters where one obtains stationary patterns, but generally a non-equidistant spacing and a finite centre of mass force is obtained, cf. figure 4.15. As above for two beam splitters, this force can be controlled via the pump power ratio to stabilize the centre of mass or induce controlled motion. Of course, the configuration not only depends on the operating conditions, but also on the initial conditions allowing a multitude of different stationary configurations.

In summary, we conclude that the particles prefer to form crystalline structures held in place by collective multiple scattering. The more particles we have, the more complex these patterns can get and the more different solutions there are. The complexity of the problem increases further, if one allows for a variation of the individual coupling parameters ζ, e.g. representing number fluctuations of the trapped atoms in a lattice or size variation of trapped beads.

Note that although appearing similar at first sight, the mechanism is different from standard optical binding of polarizable beads, which works on transverse shaping of the

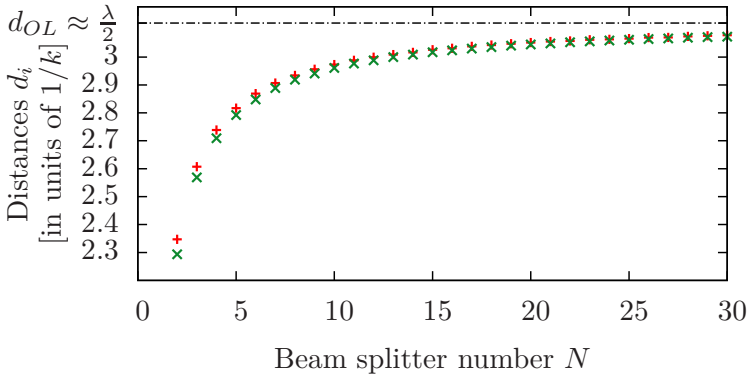

Figure 4.13: Dependence of the relative distances d_i (given in units of $1/k$) on the beam splitter number N. Symmetric parameters have been chosen, i.e. $\mathcal{P} = 1$, $k = k_y = k_z$, resulting in a equidistant lattice cf. figure 4.11. For large N we observe an asymptotic behaviour towards the expected lattice constant for a standing wave configuration, cf. equation (5.19) or [13]. For the red dots we use $\zeta = 0.01$. A small imaginary part of zeta (green dots) $\zeta = 0.01 + i0.001$ decreases the distances but still yields stable configurations (see also figure 4.8).

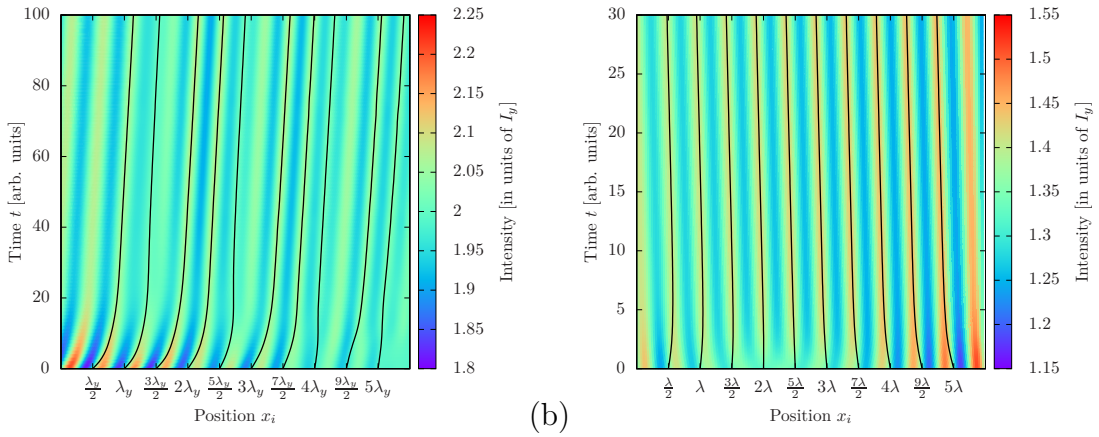

Figure 4.14: (a) Trajectories of $N = 10$ beam splitters for $\mathcal{P} = 1$, $k_z/k_y = 1.3$ and $\zeta = 0.01$. The colour coding in the background shows the change of the total field intensity $I_{tot} := I_y + I_z$ during the reorganization process of the system. The system gains a centre of mass force and the formed pattern is stable but no longer equidistant. (b) Trajectories as in (a) for parameters $\zeta = 0.01$, $\mathcal{P} = 1.3$ and $k_y = k_z$. Again there is a centre of mass force in the long time limit but the formed pattern is stable.

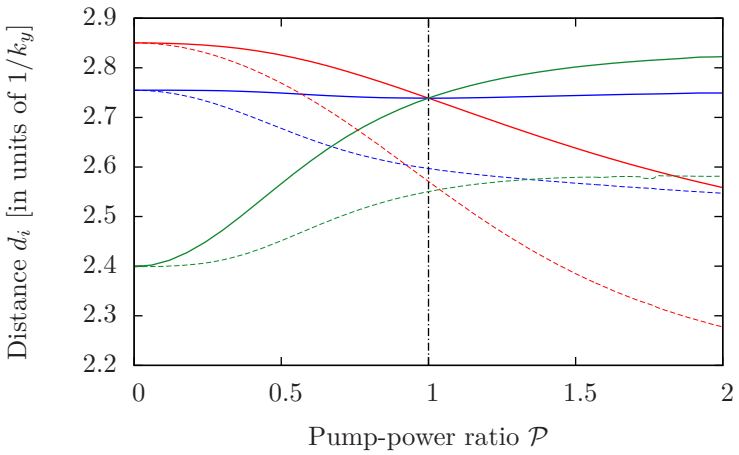

Figure 4.15: Dependence of the relative distances $d_i := x_{i+1} - x_i$ (after the system has reorganized and stabilised) on the pump-power ratio $\mathcal{P}$ for $N = 4$ particles. If we assume $k = k_y = k_z$ there is only one point ($P = 1$) where d_1 (red curve), d_2 (blue curve) and d_3 (green curve) have the same values. This corresponds to a formation of a equally spaced lattice. The dashed black lines show the relative distances for $k_z/k_y = 1.1$. In this case no stable equidistant system can be realized.

incoming light with the particles acting as small lenses [28]. We neglected transverse effects in our model from the start.

Let us finally note that the discussed results also correspond to a setup using two counter propagating beams of equal polarization, but sufficiently different frequencies, so that scattering between the different colours is suppressed. From the particle's point of view, the interference pattern of the combined fields then oscillates so rapidly that they cannot follow and the two forces stemming from the two fields can be calculated independently. Such frequency shifts are a common method to generate 3D optical lattices by using a different frequency in each dimension. But in contrast to those cases, we get a mutual interaction between the light intensities of the different frequency components here. During the evolution the spatial shifts of the beam splitters induced by one field are seen by all other fields and influences their propagation.

Chapter 5

Tailored long-range interactions in a bichromatic optical lattice

Optical lattices for ultracold atoms are an extremely well-established and controllable technology. In general, parameters are chosen in a way to avoid back-action of the particles on the fields. The underlying physics helps here to achieve this goal as particles tend to accumulate in zero force regions, where their influence on the lattice light is minimized [12, 13]. This is radically changed in an orthogonally polarized beam setup described above, where trapping forces are only created by the back-action of the particles on the two beams and interactions in the lattice occur via multiple collective scattering.

In the following chapter we will consider a second generic example to generate tailored long-range interactions in an optical lattice. In particular we study the extra forces introduced by a second perturbation field of different wavelength in a given optical lattice formed by two strong counterpropagating beams of equal wave number k and polarization $\mathbf{e}_y$, cf. figure 5.1. By adding an extra beam of different wave number k_p and polarization $\mathbf{e}_z$ we can introduce tailored perturbations and couplings, as the field gradient is generally non-zero at the positions of the original lattices sites.

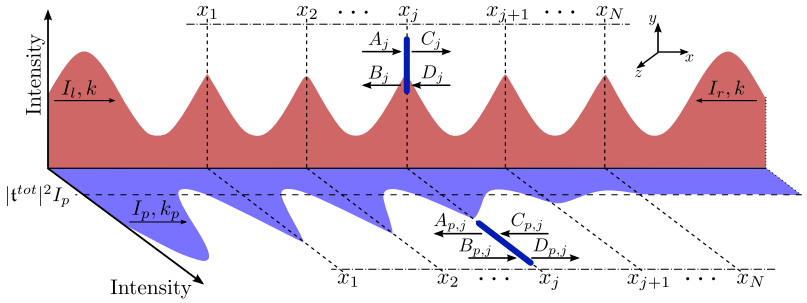

Figure 5.1: Sketch of the intensity distribution of two light fields of orthogonal polarization and different colour propagating through a 1D array of thin beam splitters. Symmetric standing wave trap (red) illuminated by an extra field with orthogonal polarization (blue).

For generality, we allow pump-power asymmetries for the dominant standing wave field $\mathcal{P} := I_r/I_l$, where the first indices l and r stand for *left* and *right* suggesting the direction of incidence. The intensity of the additional perturbation field is called I_p. The same index notation will also be used for the corresponding field amplitudes.

5.1 Single beam splitter in a bichromatic optical lattice

First we want to discuss the force onto a single beam splitter in a perturbed standing wave. The force induced by a standing wave laser field is already discussed in [13] and reads

$$\mathcal{F} = \frac{2(I_l - I_r)(|\zeta|^2 + \mathrm{Im}(\zeta))}{c|1+i\zeta|^2} + \frac{-4\sqrt{I_l I_r}\,\mathrm{Re}(\zeta)\sin(2kx+\varphi)}{c|1+i\zeta|^2} \tag{5.1}$$

$$=: \mathcal{F}_{rp} + \mathcal{F}_{dp}. \tag{5.2}$$

The first term in (5.1) corresponds to the radiation pressure where incoherent reflection is included via $|\zeta|^2$ and the second term is the dipole force whose direction is dependent on the sign of $\mathrm{Re}(\zeta)$. Due to the lack of a field intensity gradient in this case the additional force from the perturbation field contains just the radiation pressure term

$$\mathcal{F}_p = \frac{2I_p(|\zeta_p|^2 + \mathrm{Im}(\zeta_p))}{c|1+i\zeta_p|^2}. \tag{5.3}$$

We assumed $\zeta \neq \zeta_p$. The perturbation force is independent of the wavelength of the perturbation field and acts in beam direction. The total force onto a beam splitter in such a perturbed optical lattice is $\mathcal{F}_{tot} = \mathcal{F} + \mathcal{F}_p$. From this we can deduce the potential of this force via $V(x) = -\int_0^x \mathcal{F}_{tot}(x')dx'$, which leads us to

$$V(x) = -(\mathcal{F}_{rp} + \mathcal{F}_p)x - \frac{2\sqrt{I_l I_r}\,\mathrm{Re}(\zeta)}{kc|1+i\zeta|^2}\left(\cos(2kx+\varphi) - \cos(\varphi)\right). \tag{5.4}$$

As expected, the additional field induces an asymmetry of the potential. The value of this asymmetry is fixed by the sum of forces $F_{rp} + F_p$. If there is no pump asymmetry for the standing wave field the force F_{rp} is equal to zero which means that the potential asymmetry only depends on the perturbation field intensity and the matter-light interaction ζ_p. Obviously the asymmetry of the potential can be triggered by the parameters I_p and ζ_p of the perturbation field. In figure 5.2 a representative example of equation (5.4) is shown. Note that due to the asymmetry the potential depth is no longer symmetric. This can easily be understood because the potential on their right side of the beam splitter is lowered since there is less radiation pressure in the direction of the perturbation field because it counteracts the force from the trapping beam while in the other direction these forces sum up leading to a higher potential.

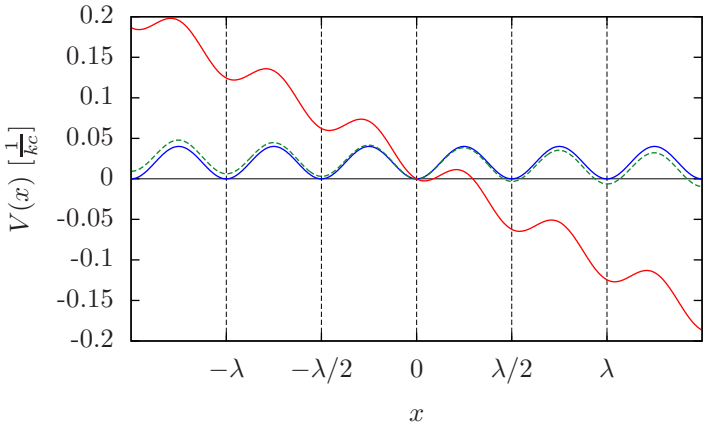

Figure 5.2: The potential given in (5.4) for different parameters. The solid, blue curve corresponds to $\zeta = \zeta_p = 0.01$ $\mathcal{P} = 1$ and $I_p = 0$. The potential gets asymmetric if the perturbation field is switched on; $\zeta = \zeta_p = 0.01$ $\mathcal{P} = 1$, $I_p = 5I_y$ (green curve) and $\mathcal{P} = 1$, $I_p = I_y$, $\zeta = 0.01$, $\zeta_p = 0.1$ (red curve). In addition the minima are shifted in this case.

The potential (5.4) has its minima at

$$x_{min} = \frac{1}{2k} \arcsin\left[\frac{c(F_{rp} + F_p)|1 - i\zeta|^2}{4\sqrt{I_l I_r}\,\mathrm{Re}(\zeta)}\right] + (2n+1)\,\frac{\lambda}{4}, \quad n \in \mathbb{Z}. \tag{5.5}$$

The minima of the potential of a perturbed optical lattice are shifted while the relative distance between two minima remains the same cf. figure 5.2.

5.2 Two beam splitters in a bichromatic optical lattice

The first relevant system to study interactions and couplings introduced by an additional field of different frequency are two beam splitters trapped at a distance d in a far detuned optical lattice at stable positions $x_1^0 = x_0 - d/2$ and $x_2^0 = x_0 + d/2$. Here x_0 denotes the stable centre of mass coordinate calculated as follows. The incident fields from left and right are assumed as $A_l = \sqrt{2I_l/c\varepsilon_0}\exp(ikx_1)$ and $D_r = \sqrt{2I_r/c\varepsilon_0}\exp(-ikx_2)$, so that the remaining amplitudes at the boundaries are $B_l = \mathfrak{r}A_l + \mathfrak{t}D_r$, $C_r = \mathfrak{t}A_l + \mathfrak{r}D_r$.

The total force onto the array of beam splitters is then given by

$$\begin{aligned}\mathcal{F}_{tot} &= \frac{\varepsilon_0}{2}\left[|A_l|^2 + |B_l|^2 - |C_r|^2 - |D_r|^2\right] \\ &= \frac{\varepsilon_0}{2}\left[|A_l|^2 + |\mathfrak{r}A_l + \mathfrak{t}D_r|^2 - |\mathfrak{t}A_l + \mathfrak{r}D_r|^2 - |D_r|^2\right],\end{aligned} \tag{5.6}$$

where the following rearrangement can be done

$$\begin{aligned}|\mathfrak{r}A_l + \mathfrak{t}D_r|^2 &= (\mathfrak{r}^*A_l^* + \mathfrak{t}^*D_l^*)(\mathfrak{r}A_l + \mathfrak{t}D_l),\\ &= |\mathfrak{r}|^2|A_l|^2 + |\mathfrak{t}|^2|D_r|^2 + \mathfrak{r}^*A_l^*\mathfrak{t}D_r + \mathfrak{r}A_l\mathfrak{t}^*D_r^*\\ |\mathfrak{t}A_l + \mathfrak{r}D_r|^2 &= |\mathfrak{t}|^2|A_l|^2 + |\mathfrak{r}|^2|D_r|^2 + \mathfrak{t}^*A_l^*\mathfrak{r}D_r + \mathfrak{t}A_l\mathfrak{r}^*D_r^*.\end{aligned}$$

This implies the following relation

$$\begin{aligned}&|\mathfrak{r}A_l + \mathfrak{t}D_r|^2 - |\mathfrak{t}A_l + \mathfrak{r}D_r|^2\\ &= |A_l|^2(|\mathfrak{r}|^2 - |\mathfrak{t}|^2) - |D_r|^2(|\mathfrak{r}|^2 - |\mathfrak{t}|^2) + (\mathfrak{r}\mathfrak{t}^* - \mathfrak{r}^*\mathfrak{t})(A_lD_r^* - A_l^*D_r),\\ &= |A_l|^2(|\mathfrak{r}|^2 - |\mathfrak{t}|^2) - |D_r|^2(|\mathfrak{r}|^2 - |\mathfrak{t}|^2) - 4\,\mathrm{Im}(\mathfrak{r}\mathfrak{t}^*)\,\mathrm{Im}(A_lD_r^*).\end{aligned} \tag{5.7}$$

Using the relations $\mathrm{Im}(A_lD_r^*) = 2\sqrt{I_lI_r}/(c\varepsilon_0)\sin(k(x2-x1))$ and $x_0 = d/2$ (assuming equal mass for both beamsplitters), the total force can be calculated as

$$\mathcal{F}_{tot} = \frac{1}{c}\left[(1 + |\mathfrak{r}|^2 - |\mathfrak{t}|^2)(I_l - I_r) - 4\,\mathrm{Im}(\mathfrak{r}\mathfrak{t}^*)\sqrt{I_lI_r}\sin(2kx_0)\right]. \tag{5.8}$$

Finding the zeros of (5.8) is straightforward and we find

$$x_0 = \frac{1}{2k}\arcsin\left[\frac{(I_l - I_r)(1 + |\mathfrak{r}|^2 - |\mathfrak{t}|^2)}{4\,\mathrm{Im}(\mathfrak{r}\mathfrak{t}^*)\sqrt{I_lI_r}}\right] + \frac{n\pi}{k}. \tag{5.9}$$

For the system of two beam splitters the reflection and transmission coefficients $\mathfrak{r}$ and $\mathfrak{t}$ of the total system derived from the total transfer matrix are

$$\mathfrak{t} = \frac{e^{ik(x_2-x_1)}}{\zeta^2\left(e^{2ik(x_2-x_1)} - 1\right) - 2i\zeta + 1}, \tag{5.10a}$$

$$\mathfrak{r} = -\frac{\zeta\left((\zeta - i)e^{2ik(x_2-x_1)} - \zeta - i\right)}{\zeta^2\left(e^{2ik(x_2-x_1)} - 1\right) - 2i\zeta + 1}. \tag{5.10b}$$

Knowing this, it is straightforward to calculate the centre of mass coordinate given in equation (5.9). The beam splitter method allows us to derive the lattice forces on the first and second particle

$$\mathcal{F}_1 = \frac{\epsilon_0}{2}\left[|A_l|^2 + |B_l|^2 - |(1 + i\zeta)A_l + i\zeta B_l|^2 - |-i\zeta A_l + (1 - i\zeta)B_l|^2\right], \tag{5.11a}$$

$$\mathcal{F}_2 = \frac{\epsilon_0}{2}\left[|(1 + i\zeta)A_l + i\zeta B_l|^2 + |-i\zeta A_l + (1 - i\zeta)B_l|^2 - |C_r|^2 - |D_r|^2\right]. \tag{5.11b}$$

The additional perturbation field is described by the perturbation amplitudes $A_p = \sqrt{2I_p/c\varepsilon_0}\exp(ik_px_1)$, $B_p = \mathfrak{r}A_p$ and $C_p = \mathfrak{t}A_p$ and generates the additional forces on each particle ($\zeta_p = k/k_p\zeta$)

$$\mathcal{F}_{1p} = \frac{\epsilon_0}{2}\left[|A_p|^2 + |B_p|^2 - |(1 + i\zeta_p)A_p + i\zeta_pB_p|^2 - |-i\zeta_pA_p + (1 - i\zeta_p)B_p|^2\right], \tag{5.12a}$$

$$\mathcal{F}_{2p} = \frac{\epsilon_0}{2}\left[|(1 + i\zeta_p)A_{p,z} + i\zeta_pB_p|^2 + |-i\zeta_pA_p + (1 - i\zeta_p)B_p|^2 - |C_p|^2\right]. \tag{5.12b}$$

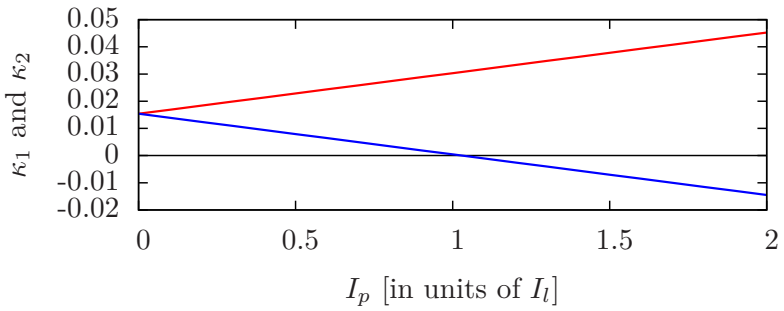

Figure 5.3: Dependence of the coupling constants κ_1 (red) and κ_2 (blue) on the perturbation field intensity $I_{p,z}$ for $\zeta = \zeta_p = 0.1$, $k = k_p$ and $\mathcal{P} = 1$. As soon as the perturbation field is switched on, the constants differ.

Here we restrict the corresponding added dynamics of the two beam splitters to small, time dependent perturbations $\Delta x_1(t), \Delta x_2(t) \ll d$ from the equilibrium positions.

Due to the fact that we assume small perturbations from the equilibrium position, the forces (5.11) and (5.12) can be linearised. This linearisation is done as follows.

The force $\mathcal{F}_1$ depends only on the positions $x_1(t)$ and $x_2(t)$ of the two beam splitters. Replacing these variables via $x_1(t) = x_0 - d/2 + \Delta x_1(t)$ and $x_2(t) = x_0 + d/2 + \Delta x_2(t)$ results in a force dependent on $\Delta x_1(t)$ and $\Delta(t) := \Delta x_2(t) - \Delta x_1(t)$. Assuming small $\Delta x_1(t)$ and $\Delta(t)$ we perform a 2D Taylor approximation to first order, resulting in

$$\mathcal{F}_1 = a + b\Delta x_1 + c(\Delta x_2(t) - \Delta x_1(t)), \tag{5.13}$$

where we defined real constants a,b and c, which are lengthy expressions depending on the system's parameters.

The same method works for the remaining forces $\mathcal{F}_2$, $\mathcal{F}_{1p}$ and $\mathcal{F}_{2p}$, where the latter two only depend on the relative distance $\Delta(t)$

$$\mathcal{F}_2 = u + v\Delta x_2 + w(\Delta x_2(t) - \Delta x_1(t)), \tag{5.14a}$$
$$\mathcal{F}_{1p} = K_{1p} + K_{2p}(\Delta x_2(t) - \Delta x_1(t)), \tag{5.14b}$$
$$\mathcal{F}_{2p} = K_{3p} + K_{4p}(\Delta x_2(t) - \Delta x_1(t)). \tag{5.14c}$$

Performing these calculations we find that some of the obtained constants are zero ($a = u = 0$) while others have the same values. We define $-K := b = v$, $\kappa_1 := K_{2p} + c$, $-\kappa_2 := K_{4p} + w$ with $c = w$ and $F_{ext} := K_{1p} = K_{3p}$. This result yields us to the following equations of motion.

$$m\Delta\ddot{x}_1(t) = -K\Delta x_1 + \kappa_1(\Delta x_2(t) - \Delta x_1(t)) + F_{ext}, \tag{5.15a}$$
$$m\Delta\ddot{x}_2(t) = -K\Delta x_2 - \kappa_2(\Delta x_2(t) - \Delta x_1(t)) + F_{ext}. \tag{5.15b}$$

The solution of the system (5.15) can be calculated analytically. First we need to find the homogeneous solution using the ansatz $\Delta x_1^H(t) = c_1 \exp(\lambda t)$ and $\Delta x_2^H(t) = c_2 \exp(\lambda t)$. Setting this ansatz into equations (5.15) results in the following linear set of equations (written in matrix notation)

$$\underbrace{\begin{pmatrix} m\lambda^2 + K + \kappa_1 & -\kappa_1 \\ -\kappa_1 & m\lambda^2 + K + \kappa^2 \end{pmatrix}}_{=:M} \begin{pmatrix} c_1 \\ c_2 \end{pmatrix} = 0. \tag{5.16}$$

The eigenvalues of the matrix M can easily be calculated and are given as $\lambda_1 = \pm i\sqrt{K/m}$ and $\lambda_2 = \pm i\sqrt{(K+\kappa_1+\kappa_2)/m}$ resulting in the eigenfrequencies $\omega_1 = \sqrt{K/m}$ and $\omega_2 = \sqrt{(K+\kappa_1+\kappa_2)/m}$. The corresponding eigenvectors are given by $\mathbf{v}_1 = (1 \;\; 1)^T$ and $\mathbf{v}_2 = (-\kappa_1/\kappa_2 \;\; 1)^T$. This results in

$$\Delta x_1^H(t) = a_1 \cos(\omega_1 t + \phi_1) - a_2 \frac{\kappa_1}{\kappa_2} \cos(\omega_2 t + \phi_2), \tag{5.17a}$$

$$\Delta x_2^H(t) = a_1 \cos(\omega_1 t + \phi_1) + a_2 \cos(\omega_2 t + \phi_2). \tag{5.17b}$$

The inhomogeneous solution can be found with the ansatz $\Delta x_1^I(t) = A$ and $\Delta x_2^I(t) = B$. Setting this into the equation and comparing the coefficients results in $\Delta x_1^I(t) = \Delta x_2^T(t) = \frac{F_{ext}}{K}$. The total solution is given as the sum $\Delta x_{1,2}^{tot} = \Delta x_{1,2}^H(t) + \frac{F_{ext}}{K}$. In compact notation this means

$$\begin{pmatrix} \Delta x_1(t) \\ \Delta x_2(t) \end{pmatrix} = \begin{pmatrix} 1 \\ 1 \end{pmatrix} (a_1 \cos(\omega_1 t + \varphi_1) + \frac{F_{ext}}{K}) + a_2 \begin{pmatrix} -\frac{\kappa_1}{\kappa_2} \\ 1 \end{pmatrix} \cos(\omega_2 t + \varphi_2) \tag{5.18}$$

with $\omega_1 = \sqrt{\frac{K}{m}}$ and $\omega_2 = \sqrt{\frac{K+\kappa_1+\kappa_2}{m}}$.

Note that the coupling constants κ_1 and κ_2 here are not necessarily equal, cf. also figure 5.3, as there is no energy conservation enforced for the motion of the two beam splitters. Since the parameters can be chosen in a way so that the coupling constant κ_1 is equal to zero, one-sided couplings can be achieved. This means that only the motion of beam splitter number two is coupled to beam splitter number one, which does not couple to the rest of the system. The direction of this effect is governed by the direction of incidence of the perturbation beam. Besides, $\kappa_2 > 0$ holds for all values of I_p, meaning that no antisymmetric modes can be obtained if $\kappa_1 < 1$, cf. (5.18). An example plot of (5.18) can be found in figure 5.4.

Generally, we find that tuning the perturbation field intensity offers a variety of different dynamics not accessible with traditional standing wave setups. This motivates a more detailed treatment of this system, using numerical methods.

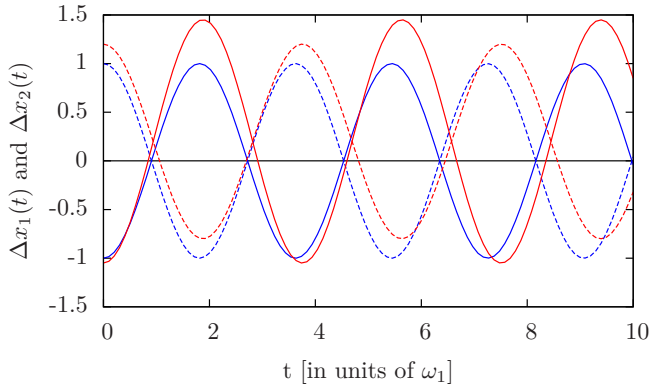

Figure 5.4: Example plot of (5.18) for $a_1 = 0$ and $a_2 = 1$ (antisymmetric mode); $\frac{\kappa_1}{\kappa_2} = 1.25$ and $F_{ext} = 0.2$ (red lines). Solid lines correspond to Δx_1 and dashed lines to Δx_2. The blue lines show the expected classical antisymmetric modes meaning that $I_{p,z} = 0$.

5.3 Many beam splitters in a bichromatic optical lattice

As shown in [13] the effective self-consistent lattice constant in a standing wave with asymmetric pump $\mathcal{A} := \frac{I_l - I_r}{\sqrt{I_l I_r}}$, with $I_l := \frac{\epsilon_0}{c}|A_l|^2$, $I_r := \frac{\epsilon_0}{c}|D_r|^2$ adjusts to

$$d_{\mathrm{sw}} = \frac{\lambda}{2}\left(1 - \frac{1}{\pi}\arccos\left[\frac{-\zeta^2\sqrt{4+\mathcal{A}^2} + \sqrt{4-\zeta^2\mathcal{A}^2}}{2(1+\zeta^2)}\right]\right). \tag{5.19}$$

In an optical lattice, multiple scattering induces long range interactions between the particles in the form of collective oscillation modes. In the self-consistent configuration the particles arrange at intensity maxima at minimal field gradients, so that this interaction is strongly suppressed for small perturbations. Adding, however, a second, perturbative field by a single running wave beam of wave number k_p injected from one side induces an additional force on each particle perturbing the regular periodic order. This perturbation then acts back on the original standing wave field. Note that a single plane wave by it self would only add a constant force, but this force is modified by multiple scattering depending on the particle distances.

As an instructive example we show these perturbing force acting on $N = 4$ beam splitters in figure 5.5. We see that the additional force is different for all the particles and changes as a function of the lattice constant relative to the wavelength of the perturbing light. Hence, by a proper choice of parameters almost any combination of magnitudes and signs of forces on the different beam splitters can be achieved.

This effect can be exploited for different purposes to control and study lattice dynamics. As a first and direct application it is possible to tailor a specific field to induce oscillations of selected particles in the optical lattice by deflecting them from their equilibrium position. As shown in figure 5.5, the force on the individual beam splitters depends

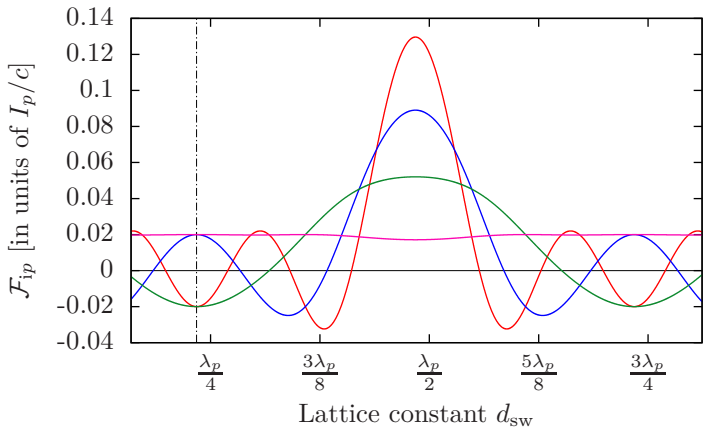

Figure 5.5: Perturbation induced force $\mathcal{F}_{ip}$ on $N = 4$ beam splitters at their unperturbed equilibrium positions in an optical lattice as function of the lattice constant d. We have set $\zeta = 0.1$, $\mathcal{P} = 1$ and $I_{p,z} = I_{l,y}$. The red line corresponds to the force $\mathcal{F}_{1p}$, the blue line to $\mathcal{F}_{2p}$, the green line to $\mathcal{F}_{3p}$ and the magenta line to $\mathcal{F}_{4p}$.

strongly on the prescribed lattice constant. This means that there is a wide range of realizable dynamics as long as the lattice constant can be tuned, cf. equation (5.19). This can be potentially refined by simultaneous use of several perturbation frequencies.

For example, using the parameters from figure 5.5 we anticipate interesting behaviour for a lattice with spacing $d_{\mathrm{sw}} \approx 0.23\lambda_p + m\pi$, $m \in \mathbb{N}$ as in that case $\mathcal{F}_{1p} = \mathcal{F}_{3p} = -\mathcal{F}_{2p} = -\mathcal{F}_{4p}$ (cf. dash-dotted line in figure 5.5). This behaviour is verified by calculating the trajectories via (4.8), the results are shown in figure 5.6. Obviously it is possible to correlate the motion of distant beam splitters in an optical lattice via the additional beam. After switching on the perturbation at $t = 0$, particles no. one and three show amplified oscillations, while the other's oscillations are damped.

In a second approach the additional field is designed to enhance interactions between selected distant areas in the lattice. As shown in figure 5.7, exciting an oscillation of one particle weakly coupled to the standing wave field will usually have little effect on the other trapped particles. But after adding a perturbation field with carefully chosen parameters, this oscillation can be transferred to the other particles, forcing them to move along. Note that due to the fact that the additional perturbation (coupling) field is imposed from only one side, this coupling effect is not symmetric and excitations can flow in a desired direction. For example, a perturbing field entering from the left hand side will maximally transfer the motion of the rightmost beam splitter. This setup allows to correlate the motion of particles and can even be used as a channel to transfer e.g. quantum information through the lattice, very much like phonons in ion crystals.

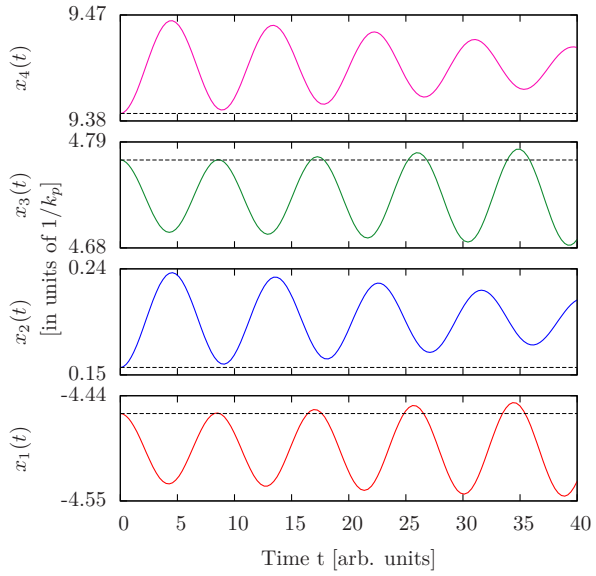

Figure 5.6: Perturbation induced motion of $N = 4$ beam splitters in a lattice due to an additional field with intensity $I_{p,z} = I_{l,y} = I_{r,y}$, wave vector $k_p = k$, $\zeta = \zeta_p = 0.1$ and damping parameter $\mu = 0.01$. The black, dashed lines show the unperturbed trapping positions $x_i = n_i d_0 - x_0$ ($n_i \in \{1, 2, 3, 4\}$) for $d_0 = 0.23\lambda_p$.

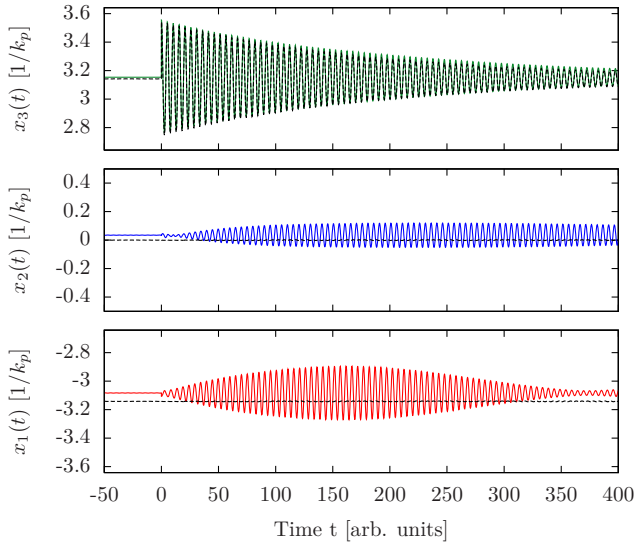

Figure 5.7: Example plot for the resonant coupling of three beam splitters, trapped in a standing wave configuration with $d_0 = \lambda_p/2$. We used $\zeta = 0.01$, $\zeta_p = 0.1$, $I_l = I_r = 20I_p$ and $k/k_p = 0.99$. The rightmost beam splitter is displaced from the equilibrium position at $t = 0$, resulting in a damped oscillation (damping parameter $\mu = 0.01$). The black curves show the resulting dynamics for $I_p = 0$. The green ($x_3(t)$), blue ($x_2(t)$) and red ($x_1(t)$) curves show the dynamics if the coupling field is switched on. Note the resonant coupling between x_1 and x_3.

Chapter 6

Conclusions

We have shown that even in the case of non-interfering counter propagating light fields of different polarization and frequency, stable lattice configurations of particles held in space by multiple coherent scattering are possible. In contrast to conventional optical lattices the light here plays a decisive dynamical role as multiple scattering is essential to form and stabilize the structure. Compared to prescribed optical lattices the physics is much closer to the case of solids, where lattice dynamics in form of phonons not only keeps the atoms in place but also mediates long range interactions. Interestingly, in conventional optical lattices such interactions can be tailored by adding additional coupling fields of suitable frequency and polarization.

While we have performed our calculations only for 1D geometries, where a semi-analytic scattering approach can be used, similar effects should be present in 3D geometries as well.

In general for very far detuned optical fields these effects will be rather small but their importance will grow with the size of the lattice as well as in transversally confined fields. Particularly strong effects can be expected in fields guided by nano optical devices such as nano fibres or hollow core fibres. Here even for a few particles strong interactions can be expected.

In this thesis we have restricted ourselves to the bichromatic case for the sake of simplicity. Nevertheless one can expect even more complex dynamics for an increasing number of input fields as the forces onto the particles show a more complex distance dependence. Note that here we have ignored any internal optical resonances of the particles. Working close to such resonances certainly should strongly increase the effects but also will complicate the analysis.

Let us finally mention here that the system does not necessarily require a fixed set of beam splitters as a starting point. As an alternative we can consider each beam splitter to be formed by a small sub ensemble of atoms in a 1D beam configuration, as it has been proposed before [12, 13]. In our case on non-interfering counterpropagating beams, one can expect that under suitable conditions the cold atoms arrange in small groups forming at local field intensity maxima [11]. Groups of atoms at certain spatial sites

then commonly form beam splitters shaping a self-consistent lattice structure.

In contrast to conventional lattices, back-action of the particles onto the fields is an essential part of the dynamics and the field thus strongly mediates collective interactions. Light scattering on one end of the lattice influences the lattice depth at the other end, which opens a completely new branch of ultracold atom optical lattice physics. Note that atoms trapped in optical resonator fields [29] exhibit similar dynamical coupling effects, but in that case the back action is strongly restricted by the resonator geometry limiting the available interaction wave vectors.

Bibliography

[1] P. W. Courteille, S. Bux, E. Lucioni, K. Lauber, T. Bienaime, R. Kaiser, and N. Piovella. Modification of radiation pressure due to cooperative scattering of light. *Eur. Phys. J. D*, 58(1):69–73, 2010.

[2] H. Bender, Ch. Stehle, S. Slama, R. Kaiser, N. Piovella, C. Zimmermann, and P. W. Courteille. Observation of cooperative Mie scattering from an ultracold atomic cloud. *Phys. Rev. A*, 82(1):011404, 2010.

[3] H. Zoubi and H. Ritsch. Hybrid quantum system of a nanofiber mode coupled to two chains of optically trapped atoms. *New J. Phys.*, 12(10):103014, 2010.

[4] E. Vetsch, D. Reitz, G. Sagué, R. Schmidt, S. T. Dawkins, and A. Rauschenbeutel. Optical interface created by laser-cooled atoms trapped in the evanescent field surrounding an optical nanofiber. *Phys. Rev. Lett.*, 104(20):203603, 2010.

[5] P. Domokos, P. Horak, and H. Ritsch. Quantum description of light-pulse scattering on a single atom in waveguides. *Phys. Rev. A*, 65(3):033832, 2002.

[6] P. Horak, P. Domokos, and H. Ritsch. Giant Lamb shift of atoms near lossy multimode optical micro-waveguides. *Europhys. Lett.*, 61(4):459, 2003.

[7] D. E. Chang, L. Jiang, A V. Gorshkov, and H. J. Kimble. Cavity QED with atomic mirrors. *New J. Phys.*, 14(6):063003, 2012.

[8] J. Lee, D. H. Park, S. Mittal, M. Dagenais, and S. L. Rolston. Integrated Optical Dipole Trap for Cold Neutral Atoms with an Optical Waveguide Coupler. *New J. Phys.*, 15(4):043010, 2013.

[9] A. Goban, K.S. Choi, DJ. Alton, D. Ding, C. Lacroûte, M. Pototschnig, T. Thiele, NP. Stern, and HJ. Kimble. Demonstration of a state-insensitive, compensated nanofiber trap. *Phys. Rev. Lett.*, 109(3):033603, 2012.

[10] D.E. Chang, J. I. Cirac, and H.J. Kimble. Self-Organization of Atoms along a Nanophotonic Waveguide. *Phys. Rev. Lett.*, 110:113606, 2013.

[11] T. Grießer and H. Ritsch. Light-Induced Crystallization of Cold Atoms in a 1D Optical Trap. *Phys. Rev. Lett.*, 111(5):055702, 2013.

[12] I. H. Deutsch, R. J. C. Spreeuw, S. L. Rolston, and W. D. Phillips. Photonic band gaps in optical lattices. *Phys. Rev. A*, 52(2):1394, 1995.

[13] J. K. Asbóth, H. Ritsch, and P. Domokos. Optomechanical coupling in a one-dimensional optical lattice. *Phys. Rev. A*, 77(6):063424, 2008.

[14] M. Sonnleitner, M. Ritsch-Marte, and H. Ritsch. Optical forces, trapping and strain on extended dielectric objects. *Europhys. Lett.*, 94(3):34005, 2011.

[15] M. Sonnleitner, M. Ritsch-Marte, and H. Ritsch. Optomechanical deformation and strain in elastic dielectrics. *New J. Phys*, 14(10):103011, 2012.

[16] S. Ostermann, M. Sonnleitner, and H. Ritsch. Scattering approach to multicolour light forces and self-ordering of polarizable particles. *arXiv:1310.6246*, 2013.

[17] J. D. Jackson. Classical Electrodynamics 3rd edn. *New York:Wiley*, 1999.

[18] J. Jahns. *Photonik*. Oldenbourg, 2001.

[19] R. Grimm, M. Weidemüller, and Y. B. Ovchinnikov. Optical dipole traps for neutral atoms. *Adv. At. Mol. Opt. Phys.*, 42:95–170, 2000.

[20] Atomic Polarizability. `http://www.photonics.ethz.ch/fileadmin/user_upload/optics/Courses/QuantumMechanicsForOptics/polarizabilities.pdf`. Accessed: 2014-01-10.

[21] A. Xuereb, P. Domokos, J. Asbóth, P. Horak, and T. Freegarde. Scattering theory of cooling and heating in optomechanical systems. *Phys. Rev. A*, 79(5):053810, 2009.

[22] André Xuereb, Peter Domokos, Peter Horak, and Tim Freegarde. Scattering theory of multilevel atoms interacting with arbitrary radiation fields. *Physica Scripta*, 2010(T140):014010, 2010.

[23] K. Jänich. *Lineare Algebra, 8.Auflage*. Springer, 2000.

[24] D. E. Chang, K. K. Ni, O. Painter, and H. J. Kimble. Ultrahigh-Q mechanical oscillators through optical trapping. *New J. Phys.*, 14(4):045002, 2012.

[25] K.-K. Ni, R. Norte, D. J. Wilson, J. D. Hood, D. E. Chang, O. Painter, and H. J. Kimble. Enhancement of mechanical Q-factors by optical trapping. *Phys. Rev. Lett.*, 108(21):214302, 2012.

[26] A. Xuereb, C. Genes, and A. Dantan. Strong coupling and long-range collective interactions in optomechanical arrays. *Phys. Rev. Lett.*, 109(22):223601, 2012.

[27] D. Grass. Optical Trapping and Transport of Nanoparticles with Hollow Core Photonic Crystal Fibers. Master's thesis, Universität Wien, 2013.

[28] K. Dholakia and P. Zemánek. Colloquium: gripped by light: optical binding. *Rev. Mod. Phys.*, 82(2):1767, 2010.

[29] H. Ritsch, P. Domokos, F. Brennecke, and T. Esslinger. Cold atoms in cavity-generated dynamical optical potentials. *Rev. Mod. Phys.*, 85:553–601, 2013.